In presenting the dissertation as a partial fulfillment of the requirements for an advanced degree from the Georgia Institute of Technology, I agree that the Library of the Institute shall make it available for inspection and circulation in accordance with its regulations governing materials of this type. I agree that permission to copy from, or to publish from, this dissertation may be granted by the professor under whose direction it was written, or, in his absence, by the Dean of the Graduate Division when such copying or publication is solely for scholarly purposes and does not involve potential financial gain. It is understood that any copying from, or publication of, this dissertation which involves potential financial gain will not be allowed without written permission.

3/17/65
b

A STUDY OF ANOMALOUS STRESS EFFECTS IN SLIGHTLY VISCO-ELASTIC FLUIDS

A THESIS

Presented to

The Faculty of the Graduate Division

by

Charles Philip Thomas

In Partial Fulfillment

of the Requirements for the Degree

Doctor of Philosophy in the

School of Engineering Mechanics

Georgia Institute of Technology

June, 1968

A STUDY OF ANOMALOUS STRESS EFFECTS

IN SLIGHTLY VISCO-ELASTIC FLUIDS

Approved:

Chairman

Date approved by Chairman: June 25, 1968

To Becky

ACKNOWLEDGMENTS

I wish to express my sincere appreciation to Professor A. W. Marris, my advisor and friend, for the cooperation and guidance he has given me.

I wish also to thank Professors Stoneking and Wood for reading and criticizing this work.

This research was partially supported by National Science Foundation Grant Number GP 2375.

TABLE OF CONTENTS

Page

ACKNOWLEDGMENTS iii

LIST OF TABLES v

LIST OF ILLUSTRATIONS vi

SUMMARY vii

LIST OF SYMBOLS ix

Chapter

I. INTRODUCTION 1

II. THEORETICAL PRELIMINARIES 7

Classical Hydrodynamics
Viscoelasticity
Conclusions

III. EXPERIMENTAL APPARATUS, MATERIALS AND PROCEDURE . . 21

Experimental Apparatus
Materials
Procedure

IV. RESULTS AND CONCLUSIONS 35

V. SUMMARY OF CONCLUSIONS AND RECOMMENDATIONS 74

Summary of Conclusions
Recommendations

Appendix

SIMPLE FLUID THEORY 76

LITERATURE CITED 93

OTHER REFERENCES 95

VITA 96

LIST OF TABLES

		Page
1.	General Data	54
2.	Experimental Data for 1000 cs Silicone Fluid	55
3.	Experimental Data for 350 cs Silicone Fluid	57
4.	Experimental Data for 100 cs Silicone Fluid	59
5.	Experimental Data for 50 cs Silicone Fluid	61
6.	Experimental Data for 10 cs Silicone Fluid	63
7.	Experimental Data for 5 cs Silicone Fluid	65
8.	Experimental Data for Mineral Oil	67
9.	Experimental Data for Cottonseed Oil	69
10.	Experimental Data for Toluene	71
11.	Reiner's Experimental Data for Toluene	73

LIST OF ILLUSTRATIONS

		Page
1.a.	Schematic Diagram of Torsional Shear Flow	6
1.b.	Schematic Diagram of Wedge Lubrication	6
2.a.	Universal Joint and Rotor	22
2.b.	Torque Meter	22
3.	Schematic Diagram of the Parallel Plate Viscometer	23
4.	$(d/R)^2$ Versus Ω^2/P for 1000 cs, 350 cs, 100 cs Silicone Fluid	40
5.	$(d/R)^2$ Versus Ω^2/P for 100 cs, 50 cs, 10 cs, 5 cs Silicone Fluid, Mineral Oil and Cottonseed Oil	41
6.	$(d/R)^2$ Versus Ω^2/P for 10 cs, 5 cs Silicone Fluid and Toluene	42
7.	$(d/R)^2$ Versus Ω^2/P for Toluene	43
8.	$(d/R)^2$ Versus Ω/P for 1000 cs, 350 cs, 100 cs Silicone Fluid	44
9.	$(d/R)^2$ Versus Ω/P for 100 cs, 50 cs Silicone Fluid, Cottonseed Oil, and Mineral Oil	45
10.	$(d/R)^2$ Versus Ω/P for 10 cs, 5 cs Silicone Oil and Toluene	46
11.	$(d/R)^2$ Versus $\mu\Omega/P$ for 1000 cs, 350 cs Silicone Fluid . . .	47
12.	$(d/R)^2$ Versus $\mu\Omega/P$ for 100 cs, 50 cs Silicone Fluid, Cottonseed Oil and Mineral Oil	48
13.	$(d/R)^2$ Versus $\mu\Omega/P$ for 10 cs, 5 cs Silicone Fluid	49
14.	$(d/R)^2$ Versus $\mu\Omega/P$ for Toluene	50
15.	$(d/R)^2$ Versus Ω^2/P for 1000 cs, 350 cs, 100 cs Silicone Fluid	51
16.	$(d/R)^2$ Versus Ω^2/P for 50 cs, 10 cs, 5 cs Silicone Fluid, Cottonseed Oil, Mineral Oil, and Toluene	52
17.	Torque Versus Shear Rate	53

SUMMARY

The purpose of this work is to investigate the visco-elastic effects of slightly visco-elastic fluids. Fluids which behave in a Newtonian manner at low rates of shear but exhibit visco-elastic response at high rates of shear are termed slightly visco-elastic. In addition the response of toluene, an ostensibly entirely Newtonian fluid, is studied to determine whether the non-linear behavior as reported by Reiner (12) was a manifestation of viscoelasticity or whether it was strictly a hydrodynamical effect.

A parallel plate viscometer which produces the torsional shear flow is used to study the fluid response. The design of the viscometer is such that the upper plate is free to move vertically and also to align itself with the lower plate. Thus, the total normal stress is equal to the weight of the upper plate. The resulting thickness of the fluid layer ranges from one ten-thousandth to one thousandth of an inch depending upon the fluid being tested.

A silicone oil is the primary test fluid. Viscosity grades of 5, 10, 50, 100, 350 and 1000 centistokes are utilized. For comparison purposes mineral oil and cottonseed oil are tested as well as toluene.

The simple fluid theory of Noll (5) is utilized as a model for the fluid. It is shown that hydrodynamic effects such as vibration perpendicular to the plane of torsion, lack of parallelism between the plates, and secondary flow are essentially negligible effects for the fluids used and the extremely thin films present. However, it is found

that one hydrodynamic effect is of significance. It s a viscous wedge lubrication effect resulting from the self-alignment feature and an inevitable lack of parallelism when dealing with such thin films.

It is found that the normal stress present for toluene is due entirely to the viscous wedge effect.

For the oils the normal stress is due to this viscous wedge effect at low rates of shear but as the shear rate is increased the visco-elastic normal stress becomes significant and dominates the lubrication effect. The point of transition from strictly a hydrodynamic effect to a dominant visco-elastic effect depends upon the viscosity of the fluid. The more viscous oils, which should possess stronger visco-elastic properties, exhibit the transition at lower shear rates than the lower viscosity fluids.

The visco-elastic response is found to depend upon the structure of the fluid.

The simple fluid theory is shown to represent these fluids very well even though high rates of shear are employed.

LIST OF SYMBOLS

Symbol	Definition
U	Velocity
u	x-component of velocity
v	y-component of velocity
w	z-component of velocity
ρ	Mass density
p	Hydrostatic pressure
$\underline{b}$	Body force per unit mass
ν	Kinematic viscosity
μ	Viscosity
Ω	Angular velocity of the rotor
d	Gap thickness
R	Radius
$\underline{T}$	Stress tensor
$\underline{1}$	Identity tensor
$\underline{\mathcal{H}}$	History functional
$\underline{F}(s)$	History of the relative deformation gradient
tr	Trace, sum of the diagonal terms of a tensor
$< >$	Physical components
$\omega(z)$	Velocity profile
κ	Shear rate
$\underline{T_E}$	Extra stress, stress due to motion
t	Present time

LIST OF SYMBOLS (Continued)

Symbol	Definition
τ	Time, $\tau \leq t$
s	$t - \tau$

CHAPTER I

INTRODUCTION

Since the earlier experiments in England during World War II on the anomalous flow properties of fuels for flame throwers and the demonstrations by Weissenberg in the late 1940's (1), there has been much experimental investigation of strongly visco-elastic fluids, such as sour milk, various paints, high polymer solutions, etc. In the last 20 years these investigations have been guided by rational theory. That is to say, the theory of such materials, initiated by Reiner (2), Rivlin (3), Rivlin and Ericksen (4) and attaining its final climax of generality in the establishment of the "Simple Fluid" by Noll (5), gave experimenters precise and exact information on what to measure in order to correlate fluids of the type postulated. In 1957 Markovitz (6), surveying the acceptable theories of viscoelasticity at that time, recognized that the visco-elastic behavior of a fluid could be classified in terms of three material functions which could be determined by force measurements in several traditional viscometric flows. He correlated his discovery with experimental results obtained using strongly visco-elastic materials (7). It was subsequently proved mathematically by Coleman and Noll (8) that, for the class of viscometric flows, fluid behavior could be classified by three material functions. Based upon this work of Coleman and Noll, Markovitz and his associates (9) at Mellon Institute initiated a systematic experimental program of correlating strongly visco-elastic behavior.

Considering the above background, one may well ask, what experimental or theoretical research can be carried out here that would be new, and not merely a weak version of the work of Markovitz? The answer to this, and indeed the motivation for this present work, is as follows. The theory of viscoelasticity mentioned above and the associated experimental work of Markovitz is centered about strongly visco-elastic liquids. Such liquids manifest anomalous flow properties which can be easily observed at low shear rates. Merrington's phenomenon (10) of the swelling of a liquid when it is extruded from a tube is apparent. With these liquids viscometric experiments are possible using viscometers with large gaps, of the width of 1/8 - 1/4 inch, at slow speeds of rotation.*

However the literature tells us that another entirely different kind of viscoelasticity occurs. This is weak viscoelasticity which manifests itself only at high shear rates. The liquids dealt with here are almost Newtonian in behavior, Newtonian in fact, for slow flows, and exhibit departure from the classical behavior only at high shear rates. These are the liquids to which this research is directed.

As far as the writer knows, S. J. Needs was the first to record this weak viscoelasticity in vegetable and mineral oils (11). He employed a parallel plate torsional viscometer and showed that when the plates were separated by a gap of a few microns the film maintained itself and supported a load without being thrown out radially. These oils exhibited a type of viscoelasticity but only when the deformation rate was sufficiently high. Under normal flows these oils behaved in a Newtonian

*This of course facilitates experimental measurements, since heating is not as great and alignment and vibration problems are easier to correct.

manner. It is in this point that we have the difference between what we have termed weak viscoelasticity and the strong and ever-present visco-elasticity being studied by Markovitz.

Reiner (12) reported the same kind of effect as that of Needs in the ostensibly entirely Newtonian liquid, toluene. Here again the cross-stress and centripetal pumping effects characteristic of visco-elastic behavior in a torsional viscometer became apparent only when the clearance between the plates was reduced to a few microns and the deformation rate was high.

If the obvious experimental difficulties associated with these measurements lead to doubts concerning their validity, one must reply that data from another area leaves little doubt as to the existence of this "weak viscoelasticity". The area to which we refer is the experimental work on anomalous response of the oils to sound waves as investigated by Barlow and Lamb (13) in London. This anomalous behavior is due to visco-elastic phenomena developing at high shear rates.

In 1949 Henniker (14) presented evidence to support his theory that "long range forces" exist. He cited many instances of clogging of capillaries, irreversible surface tension measurements and investigations such as that of Needs (11) to support his thesis that when a liquid is in contact with a metal surface, the molecular forces in the metal act upon the adjacent molecules of the liquid thereby causing them to be oriented. These oriented molecules then react on the nearby liquid molecules to give the liquid a stiffness in the immediate neighborhood* of the solid boundary.

---

*By immediate neighborhood we mean several thousand molecules, which is a fraction of a micron.

Without commenting on the validity of Henniker's conjecture, it is thought that many of the examples he cites may be a manifestation of high shear rate, weak viscoelasticity occurring in the extremely small geometrical confines of the capillaries, etc. of the systems under consideration.

This background should indicate that there is a great need for research on this "different kind" of viscoelasticity which we call weak or high shear rate viscoelasticity.

From the practical engineering standpoint of lubrication, knowledge concerning the ability of thin films of lubricants to support loads at high shear rates and the changes in the apparent viscosity at high shear rates are of the utmost importance.

The purpose of this research is to study non-linear visco-elastic effects in thin oils and possibly such effects in toluene at high shear rates.

The major aims of this work are:

1) To determine whether the non-linear behavior of toluene as reported by Reiner (12) was truly a manifestation of viscoelasticity in an ostensibly entirely Newtonian fluid at high shear rates or whether it was a strictly hydrodynamical effect.

2) To determine whether these non-linear effects depend only on the viscosity of the liquid and exist for any liquid,* i.e., to determine

*The Navier-Stokes constitutive equation is based upon the linearization of the Cayley-Hamilton expansion for the stress as a function of the deformation rate and a certain type of anomalous stress manifestation could occur at extremely high shear rates, or extremely high viscosity, even on the postulate of Stokesian fluidity without any consideration of viscoelasticity.

whether the nonlinear effects were Stokesian fluidity effects exhibited at high shear rates, or whether they were visco-elastic effects and depend upon the molecular structure of the fluid as well as the viscosity.

To this end a parallel plate viscometer was employed. Such a viscometer produces the torsional shear flow as shown in Figure 1a.

The upper plate is rotated parallel to the fixed lower plate producing a laminar shear flow in the fluid. A normal stress or cross-stress in addition to the shear stress is developed by this flow when the fluid has visco-elastic properties. See Chapter 2 for the theoretical details.

In the particular apparatus employed in this investigation the upper plate was free to move vertically. Thus the total normal stress was always equal to the weight of the rotor, and the strength of the cross-stress was indicated by the gap thickness d. Variations in the viscosity were determined by measuring the torque required to produce the flow.

It is to be emphasized that the purpose of this research was to investigate the overall non-linear behavior of several fluids and was not to determine the constitutive functions for any particular fluid.

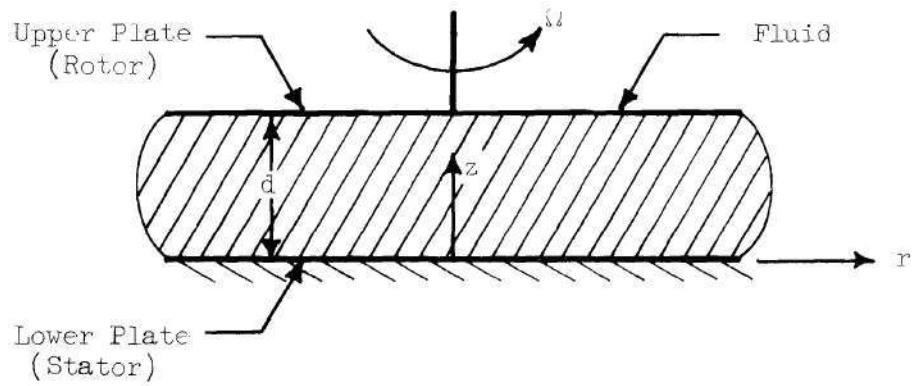

(a)

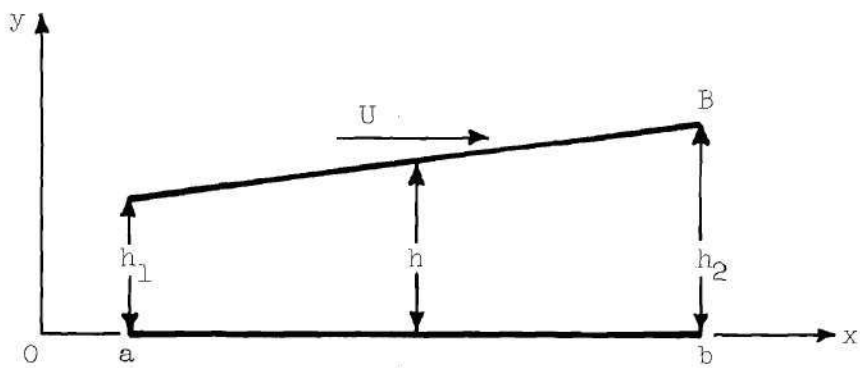

(b)

Figure 1. (a) Schematic Diagram of Torsional Shear Flow,
(b) Schematic Diagram of Wedge Lubrication.

CHAPTER II

THEORETICAL PRELIMINARIES

In analyzing the experimental data we are concerned with the occurrence of a cross-stress from two sources: Those which can be explained on the basis of classical hydrodynamics, and those due to viscoelasticity proper. These effects give basically different responses which allow them to be separated in terms of the experimental data. They are now discussed independently.

Classical Hydrodynamics

The fluids employed in this program are essentially incompressible liquids, therefore, vibration stresses and stresses due to a slight deviation from perpendicularity between the plane of torsion and the axis of rotation as considered by Taylor and Saffman (15) are unlikely to have a noticeable effect on the response of these liquids. As these authors state, normal stresses will arise, in the case of an incompressible fluid, only from geometrical imperfections which are asymmetric about every diameter, for example, a spiral groove or ridge on one of the plates. The flatness of the plates used in the present work was measured optically (See Chapter 3) and the plate surfaces were observed to be spherical in shape with a symmetrical deviation from flatness of less than 30 microinches. For the small pressures involved these liquids are considered to be incompressible. Thus, these effects are almost certainly negligible for this research.

The dynamical equations for torsional shear flow do not yield an exact solution due to the centripetal acceleration (See page 17) which can give rise to a secondary flow in the form of toroidal vorticies (16). Greensmith and Rivlin (16) investigated this secondary flow and found that its effect on the normal stress could be considered negligible for a ratio of gap thickness to radius, $\frac{d}{R}$, of 0.07. The ratio $\frac{d}{R}$ in this work varied from 1.3×10^{-5} to 6.5×10^{-4}. This ratio is several hundred times smaller than the one considered in the research of Greensmith and Rivlin due to the very thin films involved and the small radius of the plates. For this reason it is unlikely that this secondary flow will have any significant effect on the normal stresses in the present work.

While the foregoing effects will be insignificant for the reasons stated, there remains one effect which will not be small, namely the "hydrodynamic wedge effect". In spite of the self-alignment mechanism incorporated in the apparatus,* there will be both lateral motion (motion parallel to the plane of torsion) and a departure from parallelism, which, though small in absolute magnitude, becomes appreciable in relation to the film thicknesses considered.

The discussion of this effect follows the ideas first given by Rayleigh (17) for the simpler case of film flow between two rectangular plates in uniform relative motion and inclined at a small angle to each other.

---

*Chapter 3, page 21.

Consider a plate with a plane face moving with a constant velocity U.* The block is nearly parallel to another plane y = 0, which is fixed. Let the block be so wide in the z direction that the problem may be treated as two-dimensional.

Let (a,h_1); (b,h_2) be the coordinates of A, B and let (x,h) be the coordinates of any other point on AB. Since the inclination of the plane surfaces is small the velocity field is assumed to be of the form

$$u = u(x,y), \quad v = 0, \quad w = 0 \ . \tag{2.1}$$

Considering the fluid to be incompressible and assuming that the flow is steady, the continuity equation reduces to

$$\operatorname{div} \underline{v} = 0 \ . \tag{2.2}$$

Equation (2.2) is satisfied if u is a function of y only.

The governing equation of motion for the steady flow of an incompressible viscous fluid is

$$\frac{1}{\rho} \operatorname{grad} p = \underline{b} + \nu \nabla^2 \underline{v} \ , \tag{2.3}$$

where ρ is the mass density, p is the hydrostatic pressure, $\underline{b}$ is the body force per unit mass, and ν is the kinematic viscosity. Assuming the body force is equal to zero, equation (2.3) yields

$$\frac{\partial p}{\partial y} = \frac{\partial p}{\partial z} = 0 \ , \tag{2.4}$$

and

*See Figure 1b.

$$\frac{\partial p}{\partial x} = \mu \frac{\partial^2 u}{\partial y^2} . \tag{2.5}$$

Equation (2.4) implies that p is a function of x only. Thus, since u is a function of y only, equation (2.5) yields

$$\frac{dp}{dx} = \text{constant} . \tag{2.6}$$

Therefore integrating (2.5) we find that

$$\mu u = \frac{1}{2} \frac{dp}{dx} y^2 + C_1 y + C_2 . \tag{2.7}$$

The boundary conditions are

$$u = U \text{ when } y = h \text{ and } u = 0 \text{ when } y = 0 .$$

Applying these boundary conditions, equation (2.7) becomes

$$u = \frac{1}{2\mu} \frac{dp}{dx} (y^2 - hy) + \frac{Uy}{h} . \tag{2.8}$$

Since $\frac{\partial u}{\partial x} = 0$, the whole flow of liquid between 0 and h is

$$\int_0^h u \, dy = \frac{h^3}{12\mu} \frac{dp}{dx} + \frac{1}{2} Uh \equiv Q , \tag{2.9}$$

where Q is a constant. Therefore

$$\frac{dp}{dx} = \frac{6\mu U}{h^3} \left[\frac{2Q}{U} - h \right] . \tag{2.10}$$

Let $h_o = 2Q/U$, where h_o is the value of h at points of maximum

or minimum pressure. From Figure 1b we find that

$$\ell \frac{dh}{dx} = h_2 - h_1 , \tag{2.11}$$

where ℓ is the length of the plate.

Hence by (2.10)

$$\frac{dp}{dh} = \frac{6\mu U \ell}{h_2 - h_1}\left[\frac{h_o - h}{h^3}\right] , \tag{2.12}$$

and, by integration,

$$p = \frac{3\mu U \ell}{h_2 - h_1}\left\{\frac{2h - h_o}{h^2} + C\right\} . \tag{2.13}$$

Setting the pressure equal to zero beyond the ends of the block, since an addition of a constant pressure throughout the fluid will make no difference to the solution, the constants h_o and C can be determined so that $p = 0$ when $h = h_1$ and when $h = h_2$. This gives

$$h_o = 2h_1h_2/(h_1+h_2) ,$$

and

$$C = -2/(h_1+h_2) . \tag{2.14}$$

Therefore (2.13) becomes

$$p = \frac{6\mu U \ell}{h_2^2 - h_1^2}\left\{\frac{(h_1-h)(h-h_2)}{h^2}\right\} . \tag{2.15}$$

It follows that p cannot be positive unless $h_2 > h_1$.

The total pressure is given by

$$P = \int_a^b p\,dx = \int_{h_1}^{h_2} \frac{p\ell}{h_2 - h_1}\,dh$$

$$= \frac{6\mu U\ell^2}{(k-1)^2 h_1^2}\left\{\ln k - 2\,\frac{(k-1)}{(k+1)}\right\}, \qquad (2.16)$$

where $k = \frac{h_2}{h_1}$. Therefore, the total pressure P per unit width is proportional to $\mu U\ell^2/h_1^2$.

In the instrument used in this research the lateral velocity U of the rotor is proportional to the angular velocity Ω of the rotor. Since the only distance measured is the gap thickness d which is approximately equal to h_1, we find by replacing h_1 by d and ℓ by the radius R that the total load P is proportional to $\mu\Omega R^2/d^2$. The "factor of proportionality" depends upon the effective dimensions of the plates and has dimensions of length squared. Equivalently P is proportional to $\Omega R^2/d^2$, where the proportionality constant now depends upon the viscosity μ and the dimensions.

Viscoelasticity

To determine the stresses in a visco-elastic fluid subjected to the torsional shear flow we invoke Noll's theory of simple fluids. The details of this theory are included in the Appendix.

The constitutive equation of the simple fluid states that the stress tensor is determined to within a hydrostatic pressure by the

history of the relative deformation gradient.* This equation has the form

$$\underline{T} = - p\underline{1} + \overset{\infty}{\underset{s=0}{\underline{\mathcal{K}}}} (\underline{F}(s)) , \tag{2.17}$$

where p is a hydrostatic pressure, $\underline{F}(s)$ is the history and $\underline{\mathcal{K}}$ is a functional which represents the particular response a simple fluid may have. The form the functional takes depends upon the fluid.

In addition the simple fluid is assumed to be incompressible. This assumption requires that

$$\operatorname{div} \underline{v} = 0 , \tag{2.18}$$

where $\underline{v}$ is the velocity. The hydrostatic pressure p is now an indeterminate pressure. This non-uniqueness can be removed by assuming that

$$\operatorname{tr}(\underline{T} + p\underline{1}) = 0 . \tag{2.19}$$

Now p is the mean pressure, i.e.,

$$p = - \frac{1}{3} \operatorname{tr} \underline{T} . \tag{2.20}$$

The constitutive equation (2.17) must satisfy the principle of material objectivity.** This principle states that any two observers of a motion of a body find the same stress.

The steady torsional shear flow is given by the velocity field of the form

---

*See the Appendix, equation (A.5).

**See page 78, Appendix.

$$v^{<r>} = 0 , \qquad v^{<\theta>} = r\omega(z) , \qquad v^{<z>} = 0 , \tag{2.21}$$

where $\omega(z)$ is the velocity profile at a given radius r. The flow defined by (2.21) is the flow shown in Figure 1a. Equation (2.18) is satisfied by the velocity field (2.21).

For this flow the constitutive equation (2.17), restricted by the principle of material objectivity, yields the following expressions for the stresses:

$$\begin{aligned} T^{<\theta z>} &= \tau(\kappa) , \\ T^{<zz>} - T^{<rr>} &= \sigma_1(\kappa) , \\ T^{<\theta\theta>} - T^{<rr>} &= \sigma_2(\kappa) , \\ T^{<r\theta>} &= T^{<rz>} = 0 , \end{aligned} \tag{2.22}$$

where $\kappa = r\omega'(z)$.

We see that the stress system is determined by three material functions τ, σ_1, and σ_2. It is also a consequence of the principle of objectivity that τ is an odd function while σ_1 and σ_2 are even functions. Since the stresses must reduce to a hydrostatic pressure when the fluid is at rest,* $\tau(0) = \sigma_1(0) = \sigma_2(0) = 0$.

The flow of a simple fluid is governed by the dynamical equation

$$\operatorname{div} \underline{T} - \rho \operatorname{grad} \psi = \rho \underline{a} , \tag{2.23}$$

where ρ is the mass density, $\underline{a}$ is the acceleration and ψ is the potential

*This is essentially the definition of a fluid.

of the body forces, assumed to be conservative. In order for the flow assumed in (2.21) to be dynamically possible, equation (2.23) must be satisfied.

In cylindrical coordinates (2.23) takes the form

$$\frac{\partial T^{<rr>}}{\partial r} + \frac{1}{r}\frac{\partial T^{<r\theta>}}{\partial \theta} + \frac{\partial T^{<rz>}}{\partial z} + \frac{1}{r}\left(T^{<rr>} - T^{<\theta\theta>}\right) - \rho\frac{\partial \psi}{\partial r} = \rho a^{<r>} ,$$

$$\frac{\partial T^{<r\theta>}}{\partial r} + \frac{1}{r}\frac{\partial T^{<\theta\theta>}}{\partial \theta} + \frac{\partial T^{<\theta z>}}{\partial z} + \frac{2}{r}T^{<r\theta>} - \frac{\rho}{r}\frac{\partial \psi}{\partial \theta} = \rho a^{<\theta>} ,$$

$$\frac{\partial T^{<rz>}}{\partial r} + \frac{1}{r}\frac{\partial T^{<\theta z>}}{\partial \theta} + \frac{\partial T^{<zz>}}{\partial z} + \frac{1}{r}T^{<rz>} - \rho\frac{\partial \psi}{\partial z} = \rho a^{<z>} . \qquad (2.24)$$

The acceleration components are

$$a^{<r>} = -r\omega^2(z) , \qquad a^{<\theta>} = 0 , \qquad a^{<z>} = 0 . \qquad (2.25)$$

Condition (2.19) implies that the physical components of the extra stress $\underline{T}_E$, where

$$\underline{T}_E = \underline{T} + p\underline{1} , \qquad (2.26)$$

depend only on r and z since $\kappa = r\omega'(z)$. Taking gravity to be the only body force, equation (2.25) reduces to

$$\frac{\partial T_E^{<rr>}}{\partial r} + \frac{1}{r}\left(T_E^{<rr>} - T_E^{<\theta\theta>}\right) - \frac{\partial p}{\partial r} = -\rho r\omega^2 ,$$

$$r\frac{\partial T_E^{<\theta z>}}{\partial z} - \frac{\partial p}{\partial \theta} = 0 ,$$

$$\frac{\partial\left(T_E^{<zz>} - p\right)}{\partial z} - \rho g = 0 . \qquad (2.27)$$

Analyzing $(2.27)_2$, we see by assuming p to be independent of θ, that $\frac{\partial T_E^{<\theta z>}}{\partial z} = 0$. By $(2.22)_1$

$$\frac{\partial \tau(\varkappa)}{\partial z} = \frac{\partial \tau(\varkappa)}{\partial(\varkappa)} \frac{\partial(\varkappa)}{\partial z} = 0 \ . \tag{2.28}$$

Since $\frac{\partial \tau(\varkappa)}{\partial \varkappa} \neq 0$, $\frac{\partial \varkappa}{\partial z} = 0$, therefore

$$\omega(z) = cz + b \ , \tag{2.29}$$

and

$$\varkappa = cr \ , \tag{2.30}$$

where b and c are constants.

From (2.30) and (2.22) we see that the stress components depend only on r and not on z

The equations $(2.27)_{1,3}$ become

$$\frac{\partial T^{<rr>}}{\partial r} = \frac{1}{r} \sigma_2(cr) - \rho r(cz + b)^2 \ , \tag{2.31}$$

and

$$T^{<zz>} = - \rho gz + f(r) \ , \tag{2.32}$$

and must hold identically in r and z.

Assume that the flow takes place in the right circular region shown in Figure 1a. At z = 0 the disc is fixed and at z = d the disc has angular velocity Ω. Assuming adherence to the disc, the boundary conditions are

$$\omega(0) = 0 , \qquad \omega(d) = \Omega . \tag{2.33}$$

Applying (2.33) to (2.29) and (2.30) we find that

$$b = 0 ,$$

and

$$c = \frac{\Omega}{d} ; \tag{2.34}$$

hence κ, called the rate of shear, is

$$\kappa = \frac{r\Omega}{d} , \tag{2.35}$$

and

$$\omega(z) = \frac{\Omega}{d} z . \tag{2.36}$$

Since Ω is not zero and hence c is not zero, it is clear that the conditions given by (2.31) and (2.32) are incompatible with the fact that the stress components depend only on r and not on z. Hence an exact solution of (2.27) compatible with (2.33) does not exist. This difficulty disappears if the inertia and the body force in (2.31) and (2.32) are neglected.

It appears that a pure torsional shear flow is actually possible only if physically unreasonable body forces are postulated. However, for the extremely thin films considered in this experiment the potential energy gz of (2.32) is negligible compared with $T^{<zz>}$. Of lower order still is the centripetal acceleration term in equation (2.31). The

effect of this term is discussed in the first section of this chapter. It is apparent that these terms may be neglected with confidence. The following results are then obtained.

The torque M which must be applied to the discs to maintain the angular velocity Ω is given by

$$M = 2\pi \int_0^R rT^{<z\theta>}\, rdr = 2\pi \int_0^R r^2 \tau\left(r\,\frac{\Omega}{d}\right)dr \ . \tag{2.37}$$

Since $\tau(\kappa)$ is an odd function, vanishing at zero, we may write

$$\tau(\kappa) = \eta_0\kappa + \eta_1\kappa^3 + \eta_2\kappa^5 + \cdots \ , \tag{2.38}$$

where η_0, η_1, η_2 ... are material constants, with η_0 being the viscosity at zero shear rate. The torque then becomes

$$M = \frac{1}{2}\,\pi R^3\eta_0\kappa^* + \frac{1}{3}\,\pi R^3\eta_1\kappa^{*3} + \frac{1}{4}\,\pi R^3\eta_2\kappa^{*3} + \cdots \ , \tag{2.39}$$

where

$$\kappa^* = \frac{R\Omega}{d} \tag{2.40}$$

is the shear rate at $r = R$.

It follows from $(2.22)_2$ and (2.31) that the normal stress distribution at the discs is governed by the equation

$$\frac{\partial T^{<zz>}}{\partial r} = \frac{1}{r}\,\sigma_2(\kappa) + \frac{\partial\sigma_1(\kappa)}{\partial r} \ , \tag{2.41}$$

which can be written as

$$\frac{dT^{<zz>}}{dr} = \frac{d\sigma_1(\kappa)}{dr} + \frac{1}{r}\,\sigma_2(\kappa) \ . \tag{2.41}$$

Integration of (2.41) from r = 0 to r yields

$$T^{<zz>}(r) - T^{<zz>}(0) = \sigma_1(\kappa) + \int_0^{\kappa} \frac{1}{\zeta}\,\sigma_2(\zeta)d\zeta \ . \tag{2.42}$$

Assuming that the surface r = R is in contact with an atmosphere of pressure p_o, that the velocity has the form (2.21) at the edge r = R, and that interfacial effects are negligible, then

$$T^{<rr>}(R) = - p_o \ . \tag{2.43}$$

Combining (2.43) with (2.42), $(2.22)_2$ and (2.40) we obtain

$$T^{<zz>} = - p_o + \sigma_1(\kappa) - \int_{\kappa}^{\kappa^*} \frac{1}{\zeta}\,\sigma_2(\zeta)d\zeta \ . \tag{2.44}$$

Hence the total normal force N due to the normal stress $T^{<zz>}$ developed by the flow is

$$N = - \pi R^2 p_o + \frac{\pi R^2}{\kappa^{*2}} \int_0^{\kappa^*} \kappa[2\sigma_1(\kappa) - \sigma_2(\kappa)]d\kappa \ . \tag{2.45}$$

The sign of N is arranged so that the force is directed away from the flow region when N > 0.

Since $\sigma_1(\kappa)$ and $\sigma_2(\kappa)$ are even functions, vanishing at zero, we may write

$$\sigma_1(\kappa) = a_o\kappa^2 + a_1\kappa^4 + a_2\kappa^6 + \cdots \ ,$$

$$\sigma_2(\kappa) = b_0\kappa^2 + b_1\kappa^4 + b_2\kappa^6 + \cdots . \qquad (2.46)$$

Substituting (2.46) into (2.45) and integrating we find that the total normal force (which is equal to the weight of the upper plate in the viscometer used here) is proportional to $(R\Omega/d)^2$.

Conclusions

Two responses are anticipated from the preceding theoretical considerations. The classical lubrication effect is expected to be present as well as visco-elastic effects.

The lubrication theory requires the relationship between the total normal stress and $R^2\Omega/d^2$ to be linear. The visco-elastic theory based on the simple fluid model predicts that the total normal stress will be proportional to $(R\Omega/d)^2$. The lubrication effect, being a phenomenon of classical hydrodynamics will be present for all fluids but the visco-elastic effects will be present only for fluids which possess visco-elasticity.

Since the fluids employed are considered to be slightly visco-elastic and exhibit noticeable viscoelasticity only at high shear rates it is expected that the experimentally determined data will show the lubrication effect for low shear rates and then show visco-elastic effects at higher shear rates.

CHAPTER III

EXPERIMENTAL APPARATUS, MATERIALS AND PROCEDURE

Experimental Apparatus

The experimental apparatus consisted of a parallel plate viscometer and support equipment including an impedance bridge, a motor speed control, a strobatac for measuring the angular speed and reading the torque meter, a speed indicator and a liquid test call for measuring the dielectric constant of liquids. The viscometer was a modified version of the one used by Reiner for studying the cross-stress effect in the laminar flow of toluene (12).

The rotor and stator of the viscometer were hardened lapped steel plates. These plates were separated by a liquid film, a few ten-thousandths of an inch in thickness when the viscometer was in operation (See Figure 1a). The rotor turned about an axis perpendicular to the plane of the film which yielded the torsional shear flow. A ball-pivot universal joint was provided to drive the rotor. This universal joint consisted of a ball about which the rotor could freely rotate. The rotor was turned by a small pin through the ball which fitted into two slots in the rotor. (See Figure 2a). This mechanism allowed the rotor to align itself with the stator as well as move vertically.

Figure 3 shows a schematic diagram of the viscometer. The rotor (1), driven by the motor (2), was free to rotate about the ball (3) of the universal joint. A plexiglas cup (4) was attached to the stator (5) to maintain a reservoir of liquid to fill the gap. The stator was

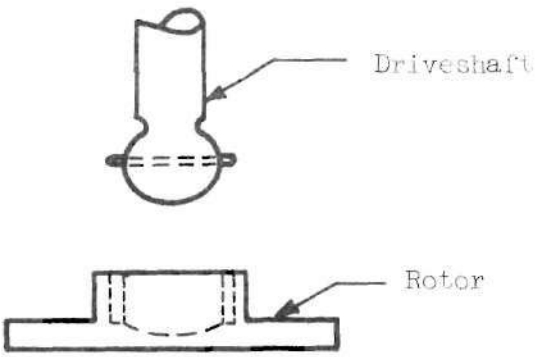

(a)

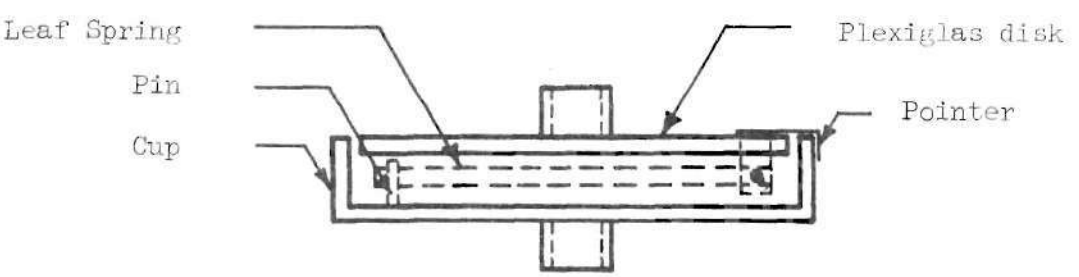

(b)

Figure 2. (a) Universal Joint and Rotor,
(b) Torque Meter.

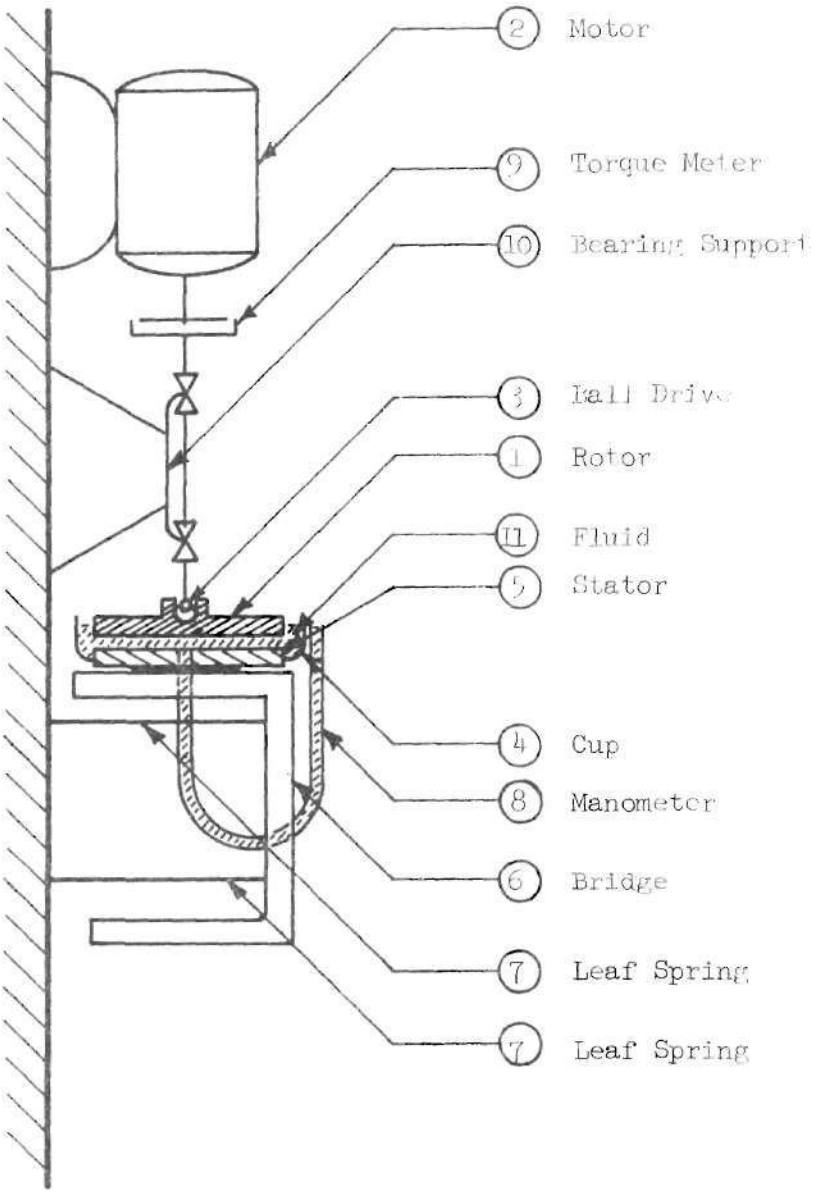

Figure 3. Schematic Diagram of the Parallel Plate Viscometer.

mounted on a bridge (6) which was supported by two leaf springs (7). A small hole was provided in the center of the stator to allow a manometer (8) to be connected or to allow a thermocouple to be positioned in the liquid gap. A mechanical torque meter* (9) was located between the bearing support (10) and the motor to measure the torque developed in the liquid film during operation of the instrument.

The viscometer was constructed so that the rotor and stator were electrically insulated from each other. Thus the upper and lower plate created a capacitor provided the liquid filling the gap was non-conducting. The fluids employed were essentially non-conducting and for such fluids the gap-thickness could then be determined by measuring the capacitance of the capacitor and utilizing the relation

$$d = \frac{0.0348\,\varepsilon\,A}{C} \qquad (1)$$

where d is the gap thickness in inches, ε is the dielectric constant of the liquid, A is the area in square centimeters and C is the capacitance in micromicrofarads (18).

An electrical connection between the rotating plate and the impedance bridge used to measure the capacitance was established by means of carbon brushes similar to those employed in small electric motors. The brushes were located directly on the driveshaft.

The rotor and stator, each 1.181 inches in diameter, were constructed of hardened, high-speed tool steel. The research of Needs (11) showed that this metal provided the best combination of working ease and

*See Figure 2b.

polishing qualities. Much care was exercised during the hardening process to insure a uniform hardness across the plates. If there was a variation in hardness across the surfaces the desired flatness of the plate surfaces could not be obtained. Also the grinding and finishing of all surfaces of the plates had to be performed after they were hardened so they would be concentric and balanced.

The surfaces of the plates which were to be in contact with the fluid were lapped until the deviation from flatness was less than 30 microinches and then they were optically polished.

The motor was a one-fifteenth horsepower reversible, variable speed d.c. motor. It was necessary to have the capability of rotating the rotor both clockwise and counterclockwise. If the alignment was perfect and the plates were perfectly flat, the results of the theory in Chapter 2 tell us that the normal stress would be identical for both directions of rotation. Thus, if the results were identical or very nearly the same, the viscometer was performing satisfactorily.

The motor was controlled by a Variac motor speed control which provided adjustable constant-speed operation of the motor for either direction of rotation. The motor could not be successfully operated below 100 rpm without additional speed reduction equipment. The speed control was a rectified power supply which allowed the speed to be varied without causing a reduction in the torque.

The torque meter consisted of a plexiglas disk to which was connected a small leaf spring, as shown in Figure 2b. The spring was inserted between two pins mounted in the bottom of the aluminum cup. This construction allowed the torque to be measured for both clockwise and

counterclockwise rotation of the rotor. A pointer on the disk indicated the deflection of the spring on a scale milled on the cup. The entire assembly rotated with the driveshaft thus making it necessary to employ a strobatac to read the meter. The torque meter also served as a vibration absorber and insulated the motor from the remainder of the viscometer.

Materials

The principal fluid employed in the investigation was a silicone polymer (Dow Corning 200 fluid) ranging in static viscosity from 5 centistokes to 1000 centistokes. For comparison purposes mineral oil and cottonseed oil were tested.

This particular silicone oil is a dimethylpolysiloxane polymer (19). It does not consist of a single molecular species but rather a statistical distribution of various molecular sizes with the average molecular weight being indicated by the absolute or static viscosity (20). The polymer is composed of long-chain molecules in a random state of orientation. At low rates of shear the tendency of these molecules to align in the direction of flow is negligible and the material will behave as a Newtonian fluid. As the shear rate is increased, the molecules begin to align themselves in an orderly fashion and the frictional resistance between adjacent layers of fluid will decrease and rigidity in the direction normal to the flow will develop. This rigidity corresponds to non-Newtonian behavior. Since the chain-length is shorter for the low viscosity fluids it is unlikely that these non-Newtonian properties will appear except at higher shear rates. For this reason, as well as the problem of viscous heating, silicone oils of relatively low viscosity

grades were selected to be used in this research.

This silicone polymer is very resistive to shear, heat and oxidation (19). Temperature changes have almost no effect on the dielectric constant of this fluid. It was essential that the fluids employed have good dielectric properties so that the film thicknesses obtained from the capacitance measurements would be accurate. Also the viscosity-temperature dependence of this silicone fluid is excellent.

Procedure

Since the purpose of this research was to investigate the non-linear behavior of slightly visco-elastic fluids, it was necessary to eliminate anything such as viscous heating which could cause the response to appear non-linear when in fact it was not.

The nature of the apparatus prohibited an external temperature control. Thus, the effect of the heating was limited by choosing working fluids which had a small viscosity-temperature dependence. Also the effect of the heating was minimized by the large mass of the metal plates with high thermal conductivity compared to the small mass of liquid. To insure that any temperature increase was known, a thermocouple was employed to measure the temperature. The viscometer was operated at high rpm only for short periods of time to assist in controlling the heating.

The viscometer was assembled and operated over the entire range of speeds without the rotor, and the residual capacitance of the instrument and the residual torque due to the bearings and contact brushes were recorded. This operation was repeated frequently to make sure that these residual readings had not changed. The residual torque and capacitance were subtracted from the data obtained from the actual tests.

Shielded cable was used to connect the impedance bridge to the viscometer to insure a constant reading of capacitance with minimum error.

At the beginning of each test the thermocouple was mounted in the small hole in the center of the stator. The plate surfaces and the inside of the cup were then cleaned with a solvent and the surfaces wiped with a camel hair brush to remove any lint and dust remaining from the cleaning. The liquid was then poured into the cup to the desired level and the rotor was gently placed over the stator. The driveshaft assembly was then inserted into place and secured and the torque meter connected to the motor. At all times extreme care was taken to keep any dirt or foreign matter from getting into the cup.

To eliminate dust and dirt from the cup during operation of the experiment the entire instrument was operated inside a wooden box with a blower attached. The blower forced filtered air into the box and out the openings, thereby, keeping dust and lint from entering. A door and two observation windows were provided for assumbling and monitoring the equipment.

After the assembly was complete the motor speed was set at approximately 400 rpm and the motor started. A quick indication of plate separation was possible from the null meter of the impedance bridge. If the plates did not separate, the motor was stopped, the plates were cleaned and new liquid was placed in the cup. If the plates were scratched they were repolished.

After the plates had separated and the thickness of the film had stabilized, the sensitivity of the impedance bridge was increased to insure an accurate reading of the capacitance. The speed was then

cautiously decreased to the lowest speed, usually 100 rpm. The capacitance and the torque were recorded after the film thickness had become stable. The speed was then increased in increments of 50 rpm with sufficient time allowed for the thickness and torque to stabilize. The time necessary for the thickness to become stable varied with the fluid being tested. For some fluids the time was a few seconds and for the more viscous ones it was a minute or more. It was necessary to have a constant speed before recording data since the solutions presented in Chapter 2 were for steady flow. The time necessary for this stabilizing effect was more critical at the higher speeds because of the viscous heating.

Therefore for speeds above 600 rpm the speed was adjusted in increments of 100 rpm and the data recorded as quickly as possible. The data recorded at each setting consisted of the torque meter reading, the temperature and the capacitance.

The viscometer was then disassembled and cleaned. A new sample of fluid was placed in the cup, the direction of rotation of the motor was reversed and an identical test was performed with only the direction of rotation changed. The film thickness and torque should have been identical for clockwise and counterclockwise rotations. Therefore, if the difference between the film thicknesses for the two directions of rotation was small, this was one indication that the results were reliable. If the difference was any appreciable amount, the alignment was checked, the plate surfaces were inspected for scratches, and the necessary corrections were made.

The data from both directions of rotation were averaged and this

Page missing from thesis

value utilized in plotting the data. Greensmith and Rivlin (16) showed in their work that the error in the normal stress due to imperfect alignment was cancelled by this averaging procedure.

It was necessary to dismantle the apparatus frequently to change the liquid and clean the plates. Also it was necessary to refinish the plates when they became scratched from repeated usage. For these reasons it was useful to have one fluid for use as a standard fluid to test the performance of the apparatus occasionally, especially following any changes in the apparatus. The 350 cs silicone fluid was used as the standard fluid. The results for this fluid were established by repeated testing until the results were repeatable from day to day and the source of any minor changes could be recognized. Once these results were established the viscometer was checked regularly using this fluid to determine whether or not it was yielding the same results.

After the results were obtained for the 350 cs silicone fluid, the remaining tests were performed using 1000 cs, 100 cs, 50 cs, 10 cs and 5 cs silicone fluid and also with mineral oil, cottonseed oil and toluene.

The liquid test cell was used in each case to determine the dielectric constant of the liquid.

Preparation of the Plate Surfaces

The successful operation of the viscometer depended largely on the plate surfaces being sufficiently flat and smooth. A technique was developed for lapping and polishing the plates which reduced the procedure to a fairly routine, although time consuming task.

The accuracy and speed with which this task could be performed

depended to a large extent on the care used in the manufacture of the plates themselves. The plates were constructed, slightly oversized, of high-speed tool steel. They were then hardened to a hardness of 55-Rockwell C to keep them from becoming badly scarred with use. All surfaces were then ground to the desired size. It was critical that a uniform hardness be obtained across the surface to be lapped. If the hardness was not uniform it was impossible to achieve the desired flatness since more metal would be removed from the softer areas resulting in a nonsymmetric surface.

Each plate was furnished with a ring two and one-half inches in outside diameter. The rings were made from the same stock material as the plates and hardened at the same time to insure that the total surface to be ground and lapped would be uniform. Each plate and ring could be screwed together and ground and lapped as one piece.

After the overall construction was completed the surfaces of the plates that were to be in contact with the fluid, with rings attached, were ground on a surface grinder to a tolerance of one ten-thousandth of an inch. The plates, with rings attached, were then hand-lapped on a bearing plate made of tool steel which had also been ground to the same tolerance. A fine grade aluminum oxide abrasive* was used as the lapping compound. It was found that the best way to achieve the desired flatness was to begin with the fine grade abrasive and then proceed directly to the polishing compounds.

The plates with rings attached were hand-lapped on the bearing plate utilizing a figure eight pattern until a majority of the grinding

*Carborundum Finishing Compound, fine grade.

marks had been removed. This procedure yielded a slightly convex shape to the surface of the plate. After both plate-ring assemblies had reached about the same stage, they were then lapped together using a circular motion while rotating both plates slowly. In this manner the higher center portions were removed yielding a flatter surface than could be obtained by lapping entirely on the bearing plate. Extreme care was taken to keep any grit from getting into the lapping compound and scratching the surfaces.

After all grinding marks were removed the surfaces would be very nearly flat, including the edges. The rings were then removed and an aluminum oxide powder of extra fine grade (600 grit) was used to begin the polishing process. This extra fine grade powder was suspended in a cutting oil, which was filtered to remove any foreign matter. It was necessary to remove the rings at this stage since it was impossible to remove all of the grit trapped in the threads otherwise. Since very little metal would be removed during the polishing process the edges did not become rounded to any appreciable extent although the rings had been removed.

The plates were lapped together using this extra fine compound until a scratch-free surface was obtained. The plates were then cleaned and polished again using an alumina polishing powder with a particle size of 0.3 microns on single-weight photographic paper, emulsion side down. The soft nap cloths commonly used with this type abrasive had a tendency to remove the inclusions in the metal and keep the surface from being smooth. However, to achieve a high luster the plates were polished briefly using a cloth and the alumina powder.

The plates were then checked for flatness using an optical flat with a helium light source. A maximum deviation from flatness of 30 microinches was allowed. This tolerance was approximately equivalent to the one micron tolerance allowed by Reiner in his research with toluene. This 30 microinch variation had to be symmetric as mentioned before, or it was rejected and the entire finishing process was repeated.

CHAPTER IV

RESULTS AND CONCLUSIONS

On the basis of the theoretical considerations presented in Chapter 2 we should expect the experimental data to show a viscous wedge effect superimposed on the visco-elastic effect. The theory of wedge lubrication requires that $\left(\frac{d}{R}\right)^2$ be proportional to $\frac{\Omega}{P}$ where P is the weight of the rotor. Simple fluid theory predicts that normal stresses due to visco-elastic effects are of the form $\left(\frac{d}{R}\right)^2$ proportional to $\frac{\Omega^2}{P}$. It is apparent that it is possible to delimit these two effects by plotting the experimental data according to these two laws.

The experimental data is recorded in Tables 1-11 and is presented graphically in Figures 4-17.

An inspection of the curves, with the possible exception of toluene, reveals the following:

1) For $\Omega < \Omega_o$, the relationship between $\left(\frac{d}{R}\right)^2$ and $\frac{\Omega}{P}$ is linear.

2) For $\Omega > \Omega_o$, the relationship between $\left(\frac{d}{R}\right)^2$ and $\frac{\Omega^2}{P}$ is linear and the relationship between $\left(\frac{d}{R}\right)^2$ and $\frac{\Omega}{P}$ is non-linear. Ω_o is the angular velocity at which the visco-elastic effect begins to develop.

The linear relationship between $\left(\frac{d}{R}\right)^2$ and $\frac{\Omega}{P}$ is exactly what is anticipated from the theory of wedge lubrication discussed previously.

The linear relationship between $\left(\frac{d}{R}\right)^2$ and $\frac{\Omega^2}{P}$ occurring at the higher shear rates* is exactly what is anticipated by Noll's simple fluid theory.

*See Tables 2-11.

We conclude that two effects are at work. At the lower shear rates there is a viscous wedge effect which is due to the lack of parallelism which occurs with such small gaps, while at higher shear rates nonlinear visco-elastic effects come into play and dominate this hydrodynamical effect.

With respect to the ostensibly Newtonian fluid toluene, some doubt must remain as to whether visco-elastic effects occur. Reiner has claimed that his results for toluene indicated the cross-stress effects of visco-elasticity. However his results shown in Figure 9 indicate that he found a linear relationship between $\left(\frac{d}{R}\right)^2$ and $\frac{\Omega}{P}$, the relationship that is predicted by lubrication theory. The data taken by the author, while deviating from Reiner's results slightly, also exhibits a linear relationship between $\left(\frac{d}{R}\right)^2$ and $\frac{\Omega}{P}$. The same experimentally determined data plotted in Figure 6 and to a much larger scale in Figure 10, gives some indication that at very high shear rates the data obtained by the author shows a linear relationship between $\left(\frac{d}{R}\right)^2$ and $\frac{\Omega^2}{P}$. While this may indicate some tendency for viscoelasticity in toluene, it is certainly not conclusive. This linear relationship between $\left(\frac{d}{R}\right)^2$ and $\frac{\Omega^2}{P}$ occurs at very high values of Ω which increases the possibility of deviations due to vibration of the viscometer.

Wedge lubrication theory indicates that if $\left(\frac{d}{R}\right)^2$ is plotted versus $\frac{\mu\Omega}{P}$, where μ is the static viscosity, the proportionality constant will depend on the dimensions of the plates and should be the same for all fluids. Thus, the slope should be the same when the data is plotted in this manner. The resulting curves, given in the Figures 11-14 show that this is not true for all the fluids. However the slope is very nearly

the same except for the 1000 cs and 350 cs silicone fluid. This reveals that the lubrication effect is being reinforced more strongly by the visco-elastic stress even at the lower shear rates for these fluids. Also, the gap thicknesses are larger for the higher viscosity fluids which causes the effective dimensions involved in the proportionality factor to vary from one fluid to another.

We observe that if the curves are extrapolated to the origin they will not pass through the origin as we might expect. This is explained by the fact that d is the mean film thickness which is calculated from the capacitance and not the actual film thickness. The actual film thickness would have a small variation due to the plates not being perfectly flat. Thus, it is reasonable for the curves to pass through some point other than the origin. However, the value of d obtained from extrapolating to the origin should be very small, which it is in every case.

The value of the shear rate at which the transition from primarily a lubrication effect to a dominant visco-elastic effect occurs increased as the viscosity decreased (See Figures 4-9 and Tables 2-11). The transition is shown more clearly in Figures 15 and 16 where the data is presented in a semi-log plot.

The data for cottonseed oil and mineral oil, presented in Figures 5 and 8, indicates that the visco-elastic effect depends upon the structure as well as the static viscosity of the fluid. The cottonseed oil (viscosity, 59 cs at $77^{\circ}F$) exhibits a stronger hydrodynamic wedge effect than the 50 cs silicone fluid, which it should since it has higher viscosity. However at the higher shear rates it has a weaker visco-elastic

effect than the less viscous 50 cs silicone fluid. The response of the mineral oil (viscosity, 89 cs at 77°F) when compared to the response of the 100 cs and 50 cs silicone fluid exhibited a weaker visco-elastic effect than the silicone fluids.

The fact that the viscosity of these vegetable oils is more temperature sensitive cannot account for the observed behavior since the temperature increase was only 3°F to 5°F (See Tables 9 and 10) which would not produce the observed results. Thus it is apparent that viscoelasticity of a fluid depends on the molecular structure as well as the viscosity.

Fluctuations observed in the experimental data are believed to be caused by viscous heating effects which are present for the higher viscosity fluids. Because of the large mass of the viscometer the heat generated in the liquid film would be dissipated rapidly to the atmosphere due to the high conductivity of the metal. Thus, the results should not be seriously affected by the viscous heating. Effects of this heating are also reduced by the flat temperature-viscosity curve characteristic of the silicone fluids.

Considering these facts, the heating present should not cause the conclusions to be incorrect even for the 1000 cs silicone fluid where the temperature increase was measured to be 15°F. There was almost no increase in temperature for the 10 cs and 5 cs silicone fluid and no measurable increase for toluene.

The data obtained from the torque measurements is plotted in Figure 17 as torque versus shear rate. The torque measurements were not completely satisfactory due to the accuracy not being great enough to

give reliable results for the 5 cs and 10 cs silicone fluid and toluene. Nevertheless, the results indicate the non-linear effects predicted by the simple fluid theory.* Fluctuations present were a result of viscous heating and the fact that the resisting torque caused by the brushes varied during operation of the viscometer. The deviation from linearity occurs at shear rates somewhat higher than the shear rates at which the visco-elastic normal stress appeared. This is reasonable since the first non-linear term in the torque is a cubic as compared to a second order term for the normal stress. See equations (2.39) and (2.46) of Chapter 2.

Curves prepared by the manufacturer (19) showing the apparent viscosity of the silicone fluids indicate that the values of the shear rate for which the apparent viscosity begins to decrease correspond closely with the values of the shear rate for which the torque curves in Figure 17 become non-linear.

Torque data presented for cottonseed oil and mineral oil shows that the non-linear effects in the shear stress depend on the molecular composition of the fluid as well as the viscosity. This is in agreement with the similar conclusion in regard to the cross-stresses.

*Equation (2.39) of Chapter 2.

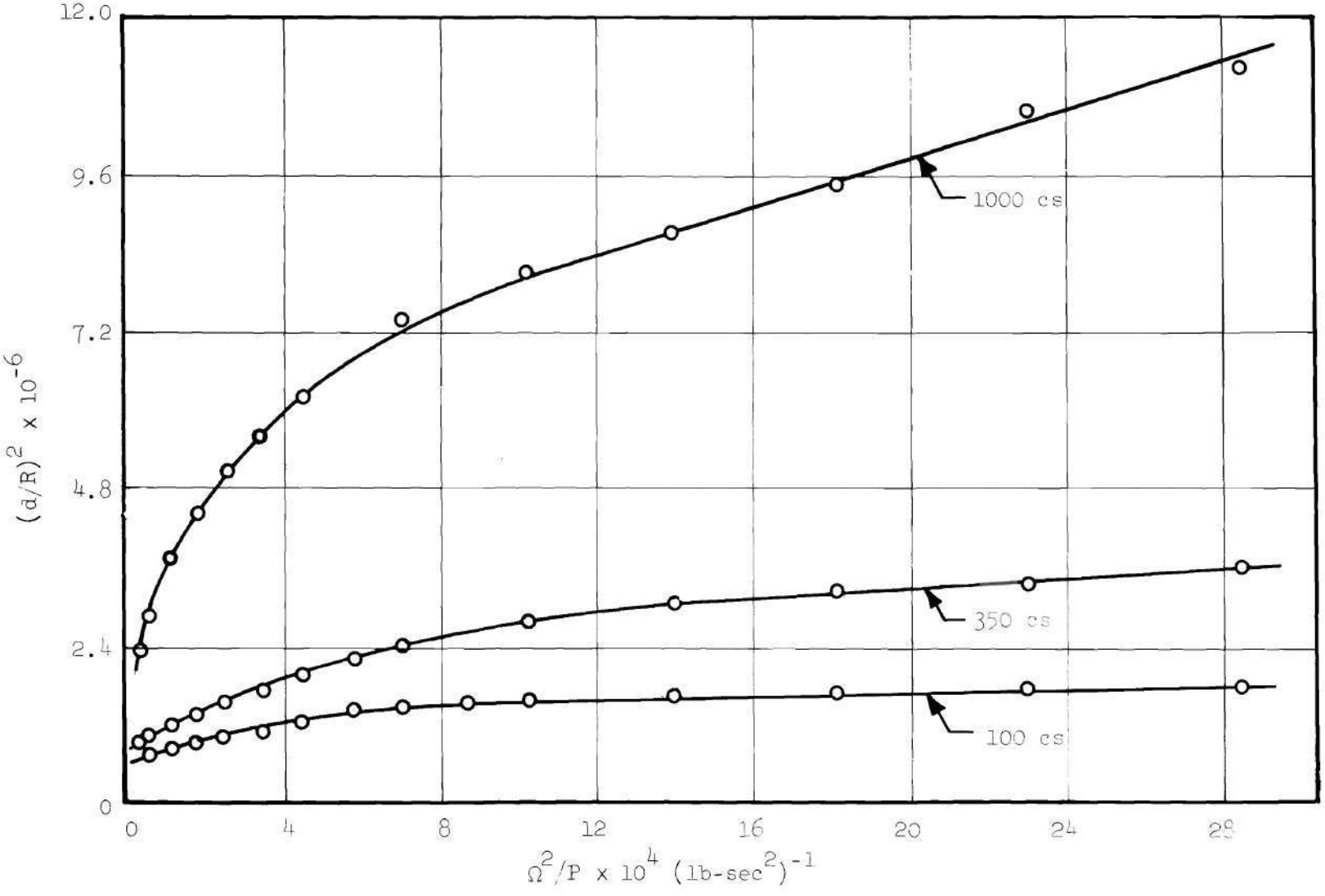

Figure 4. $(d/R)^2$ Versus Ω^2/P For 1000 cs, 350 cs, 100 cs Silicone Fluid.

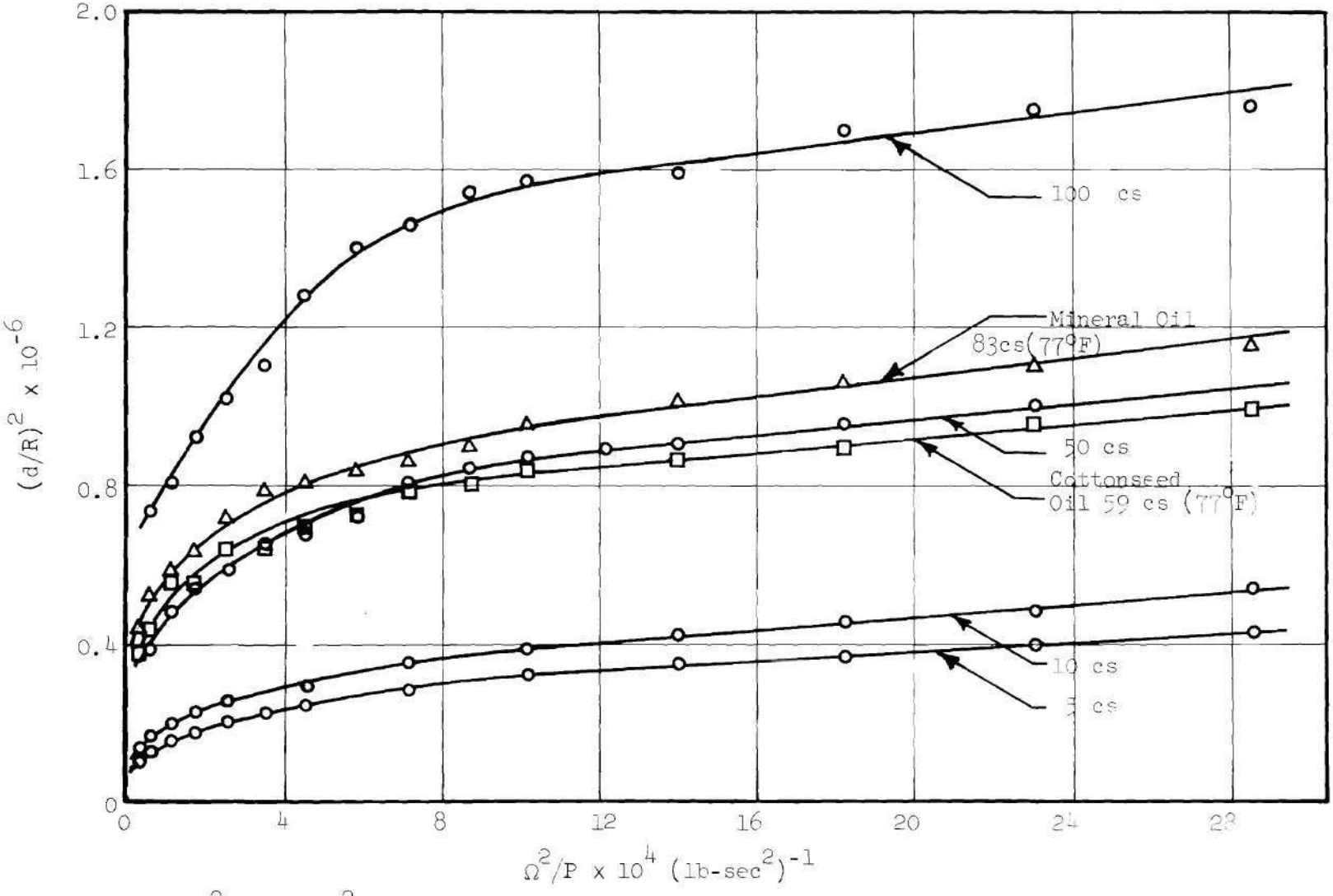

Figure 5. $(d/R)^2$ Versus Ω^2/P For 100 cs, 50 cs, 10 cs, 5 cs Silicone Fluid, Mineral Oil and Cottonseed Oil.

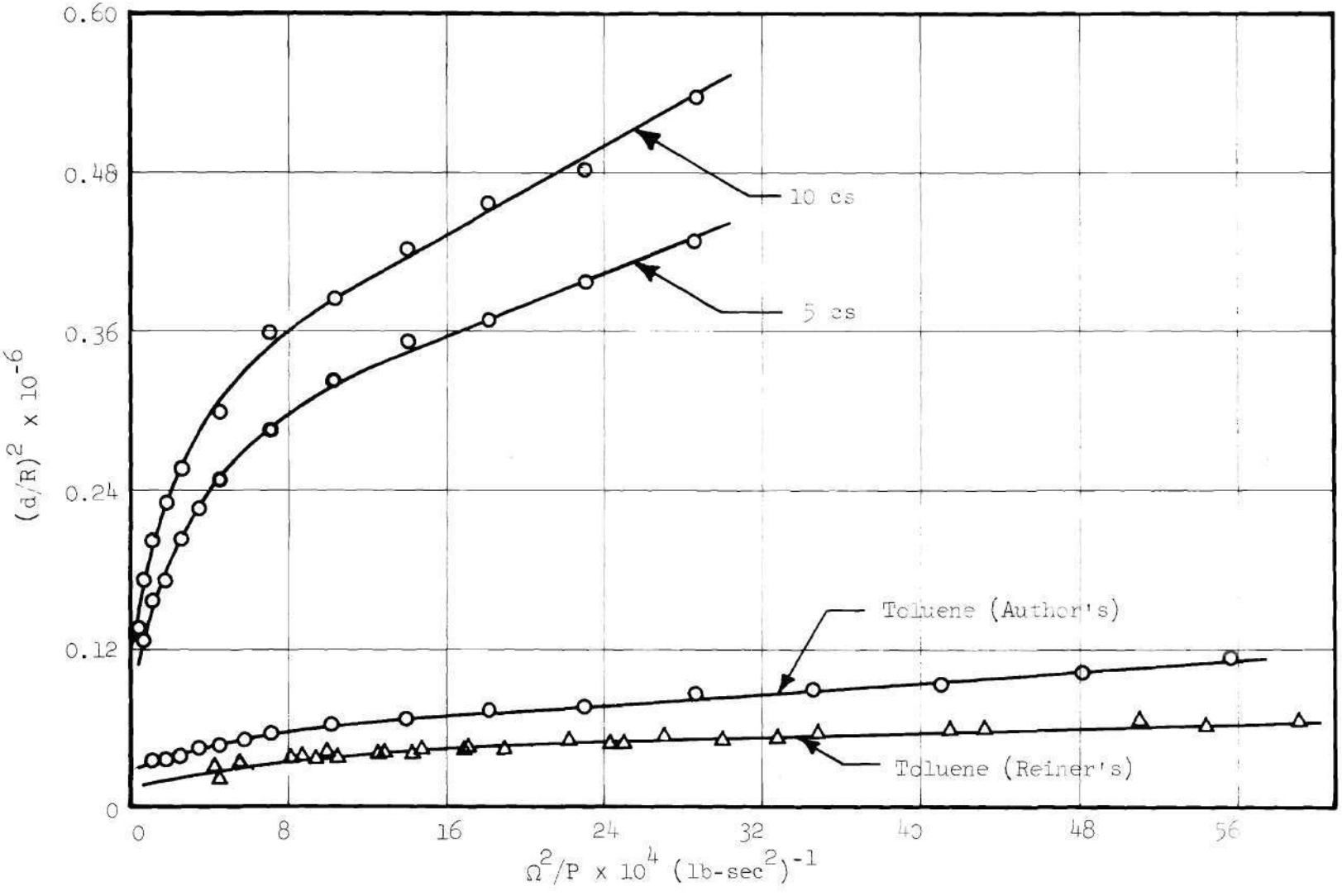

Figure 6. $(d/R)^2$ Versus Ω^2/P For 10 cs, 5 cs Silicone Fluid and Toluene.

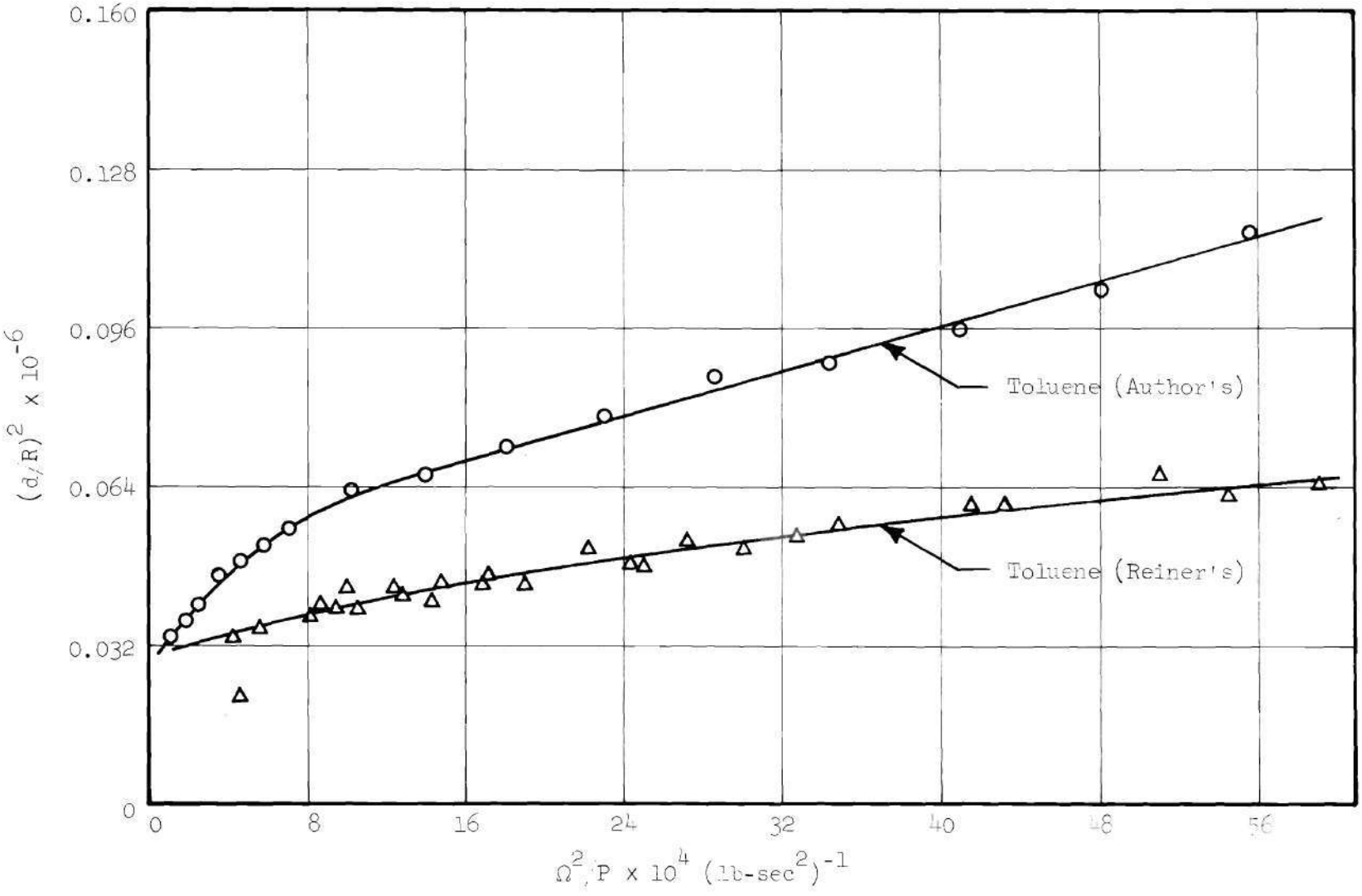

Figure 7. $(d/R)^2$ Versus Ω^2/P For Toluene.

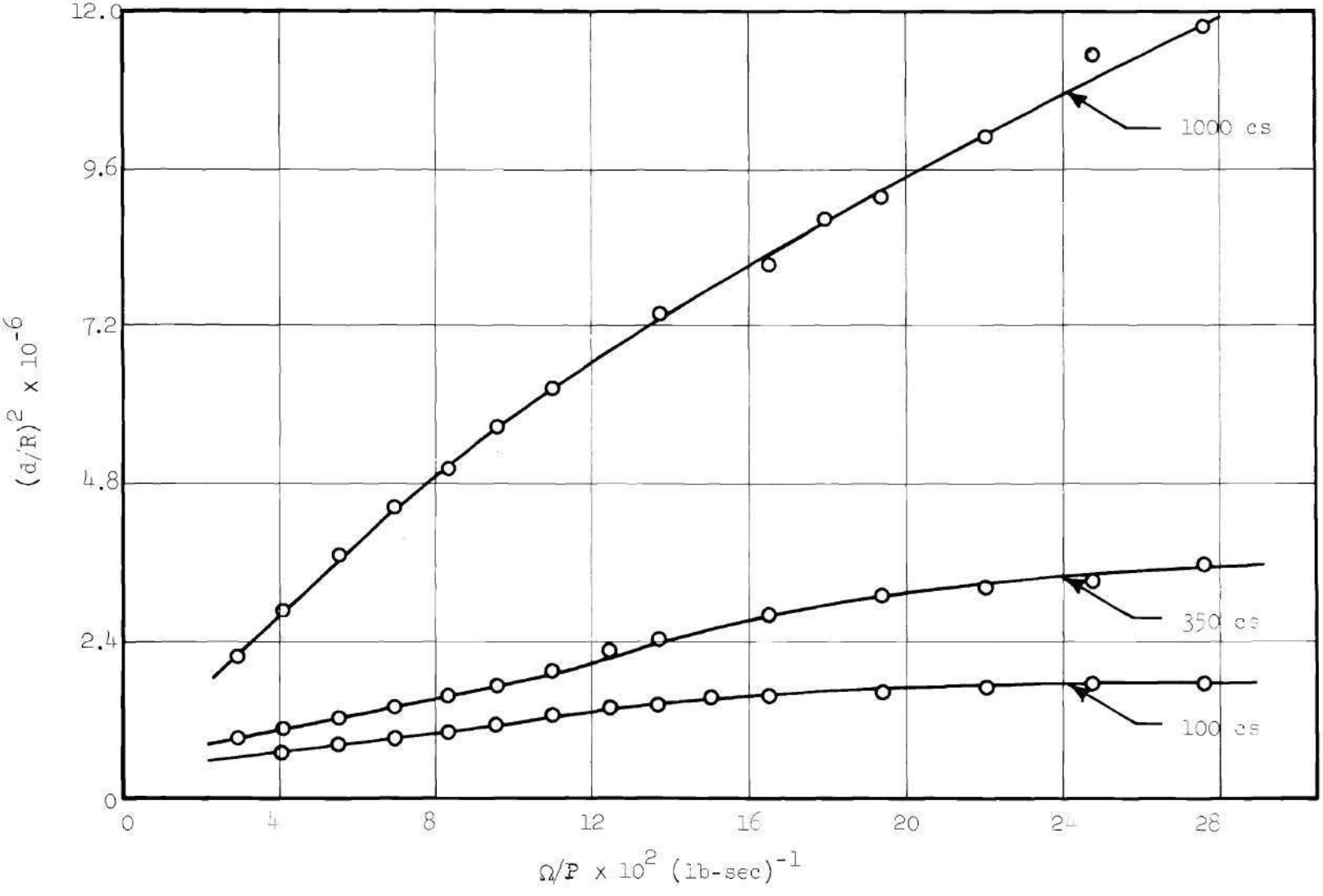

Figure 8. $(d/R)^2$ Versus Ω/P For 1000 cs, 350 cs, 100 cs Silicone Fluid.

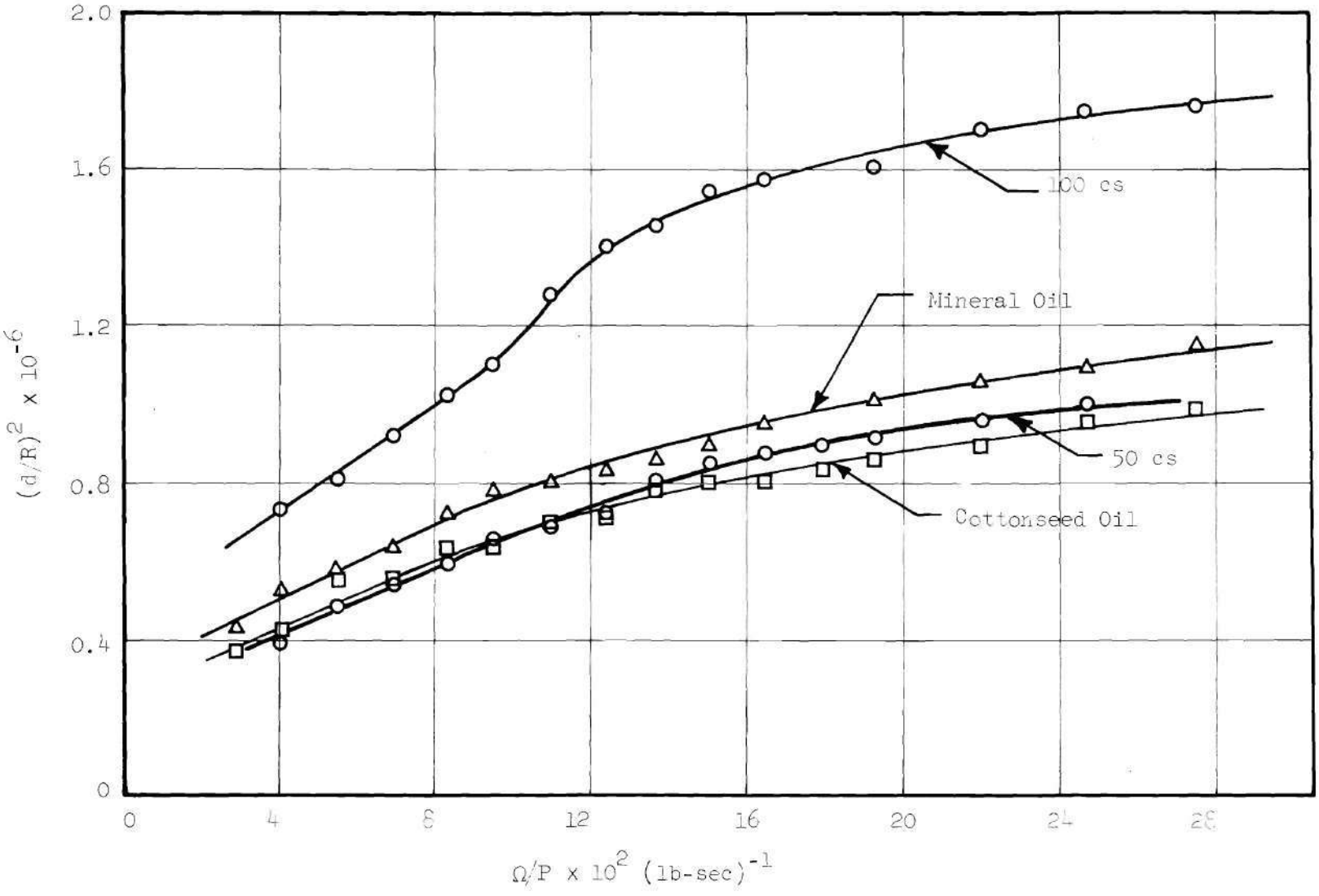

Figure 9. $(d/R)^2$ Versus Ω/P For 100 cs, 50 cs Silicone Fluid, Cottonseed Oil, and Mineral Oil.

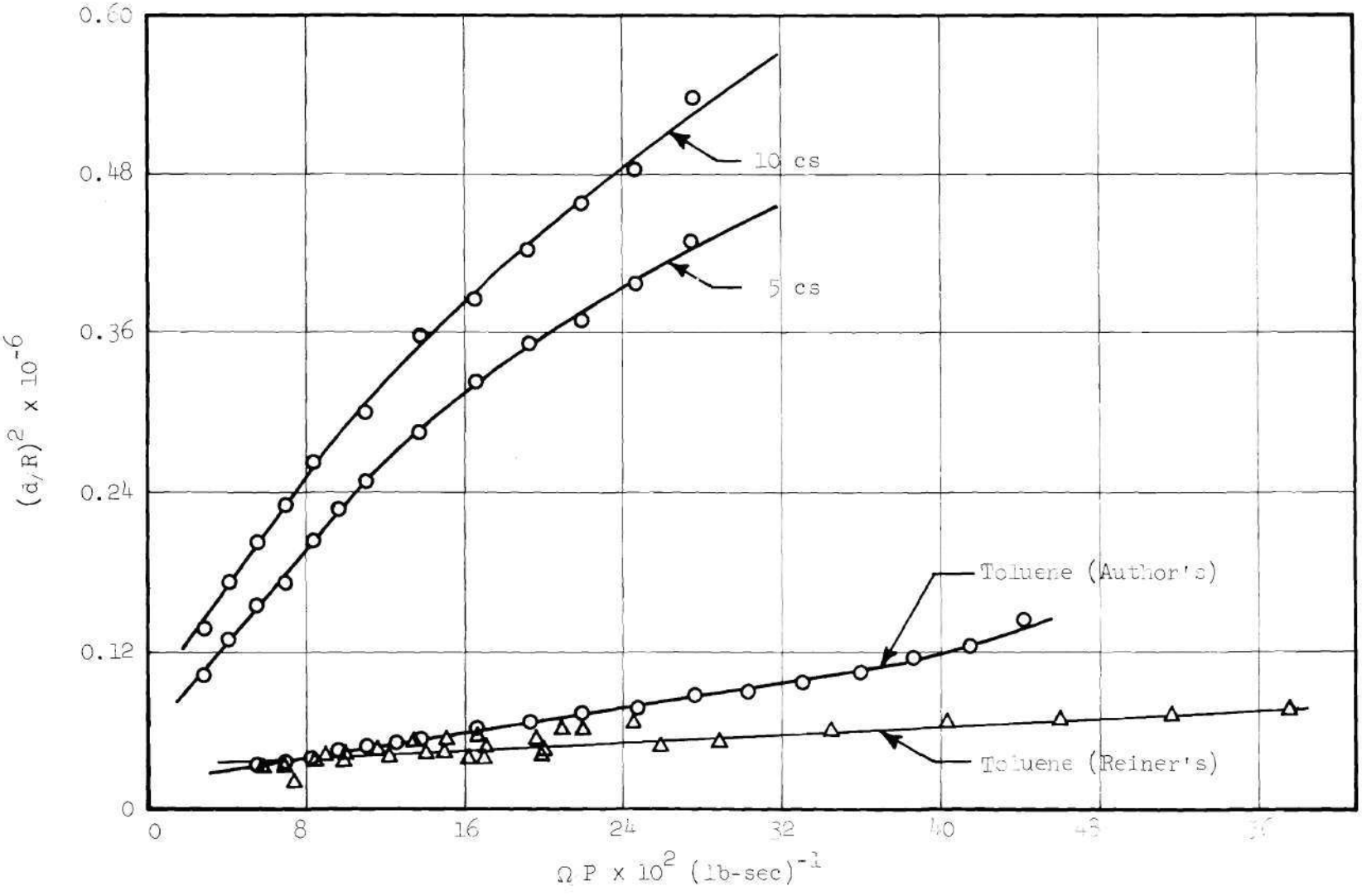

Figure 10. $(d/R)^2$ Versus ΩP For 10 cs, 5 cs Silicone Oil and Toluene.

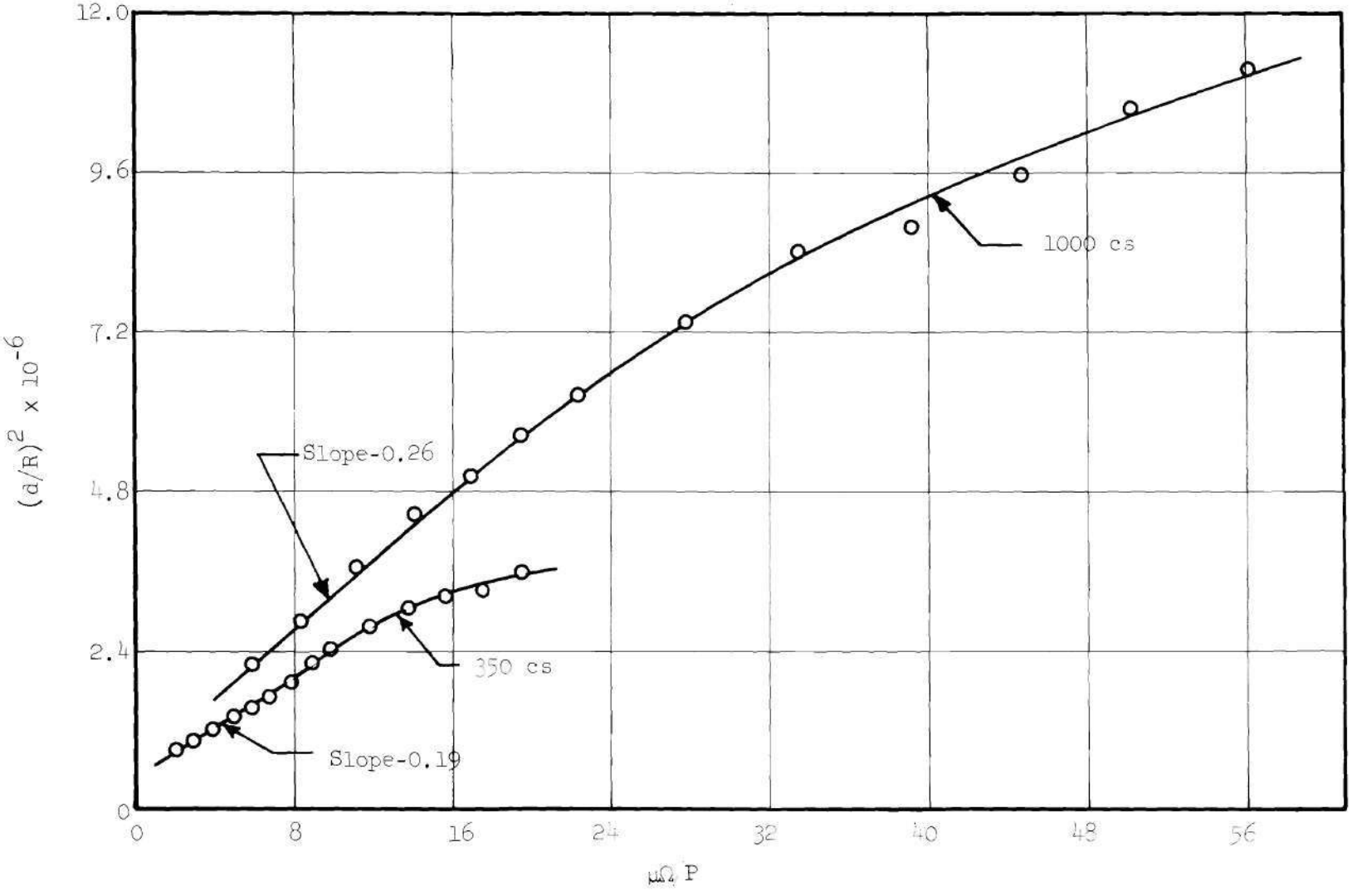

Figure 11. $(d/R)^2$ Versus $\mu\Omega/P$ For 1000 cs, 350 cs Silicone Fluid.

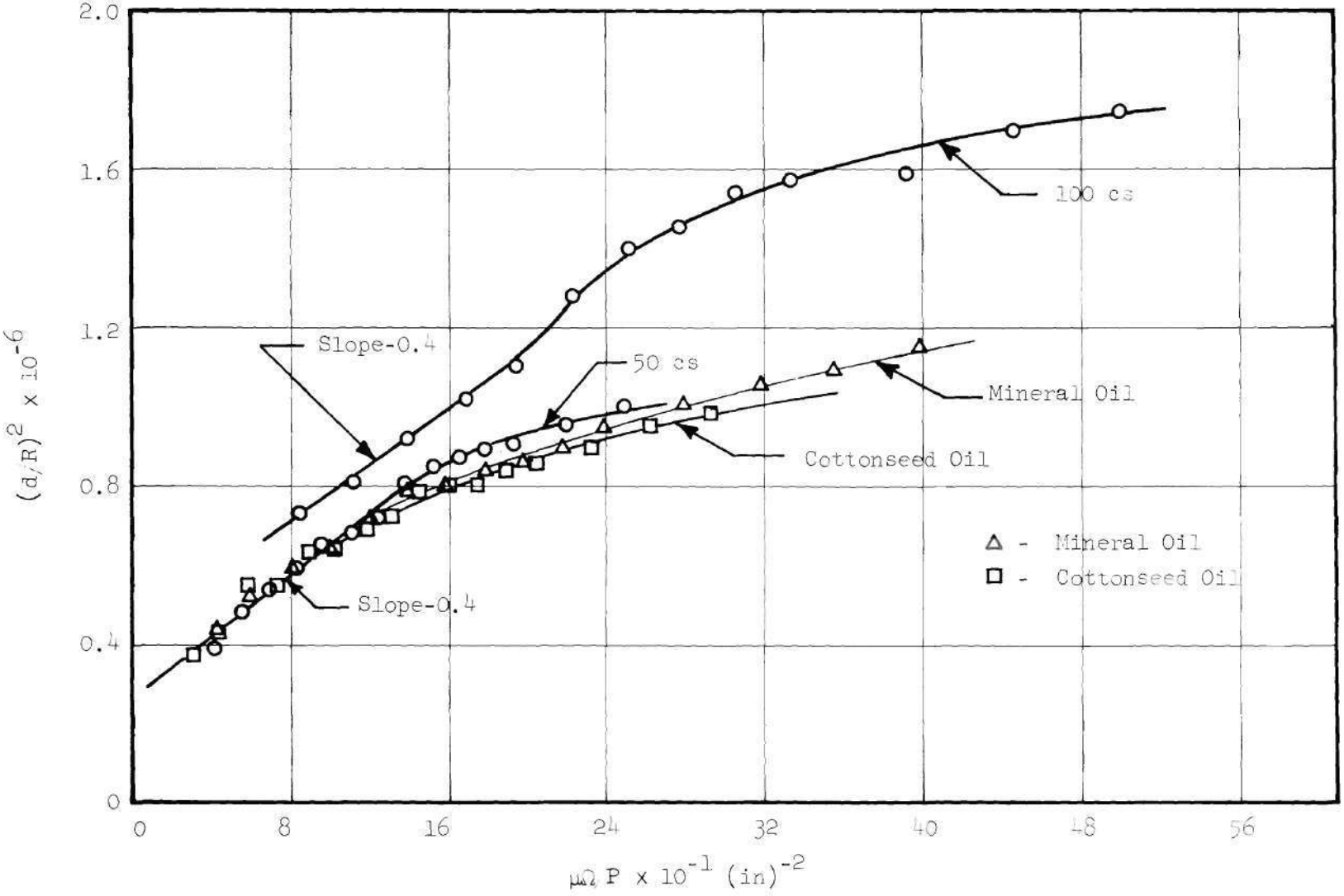

Figure 12. $(d/R)^2$ Versus $\mu\omega P$ For 100 cs, 50 cs Silicone Fluid, Cottonseed Oil and Mineral Oil.

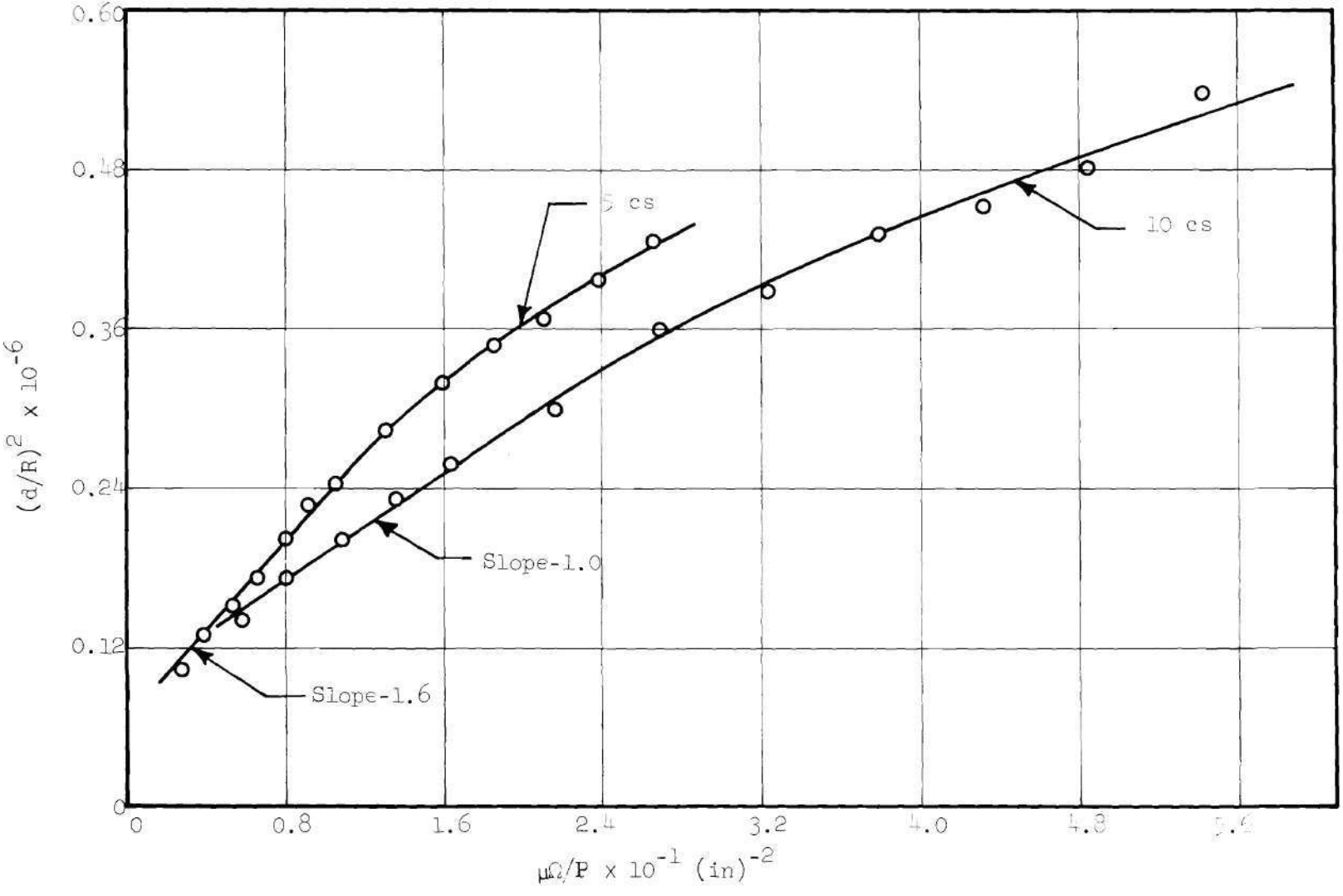

Figure 13. $(d/R)^2$ Versus $\mu\Omega/P$ For 10 cs, 5 cs Silicone Fluid.

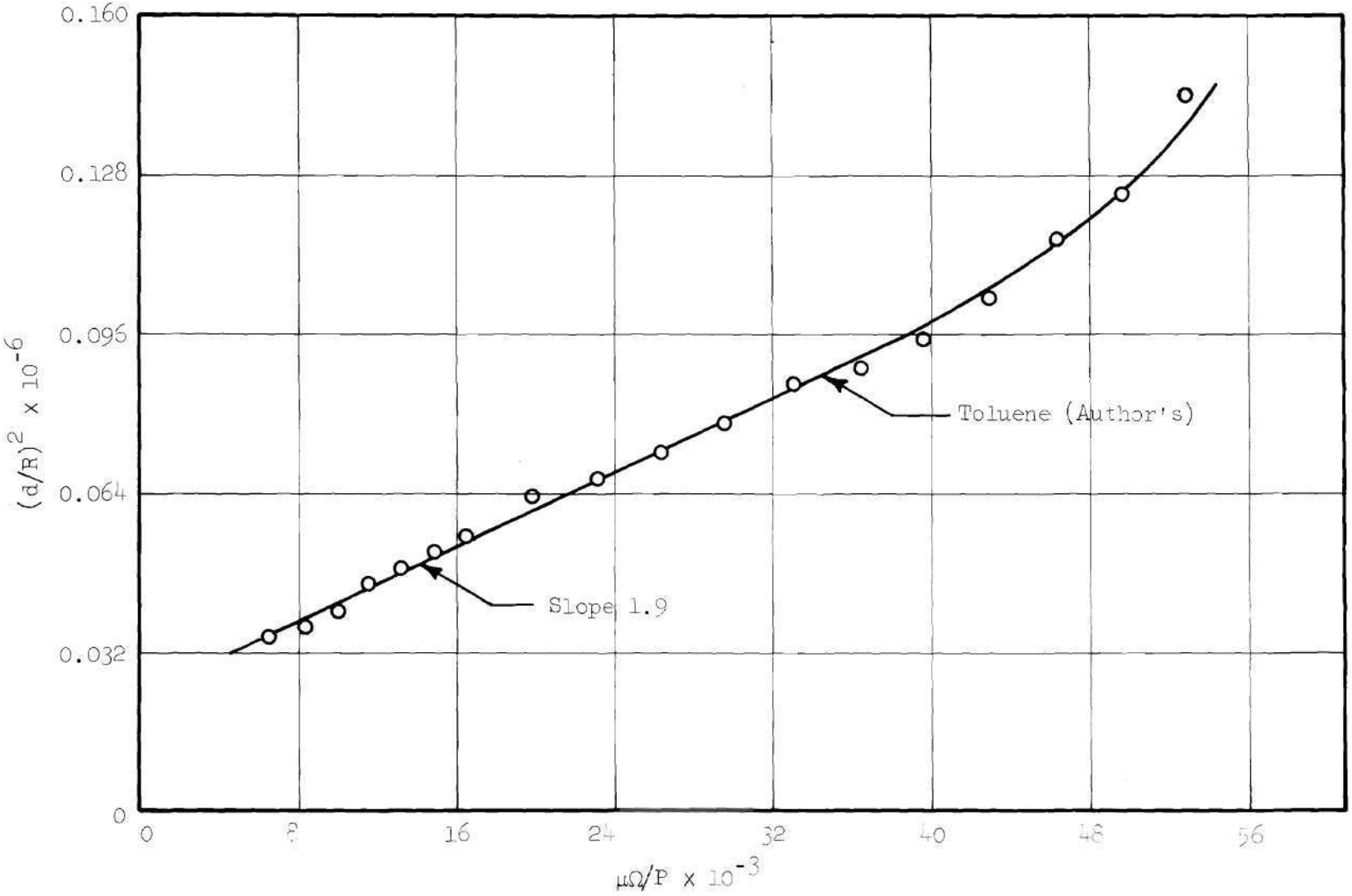

Figure 14. $(d/R)^2$ Versus $\mu\Omega/P$ For Toluene.

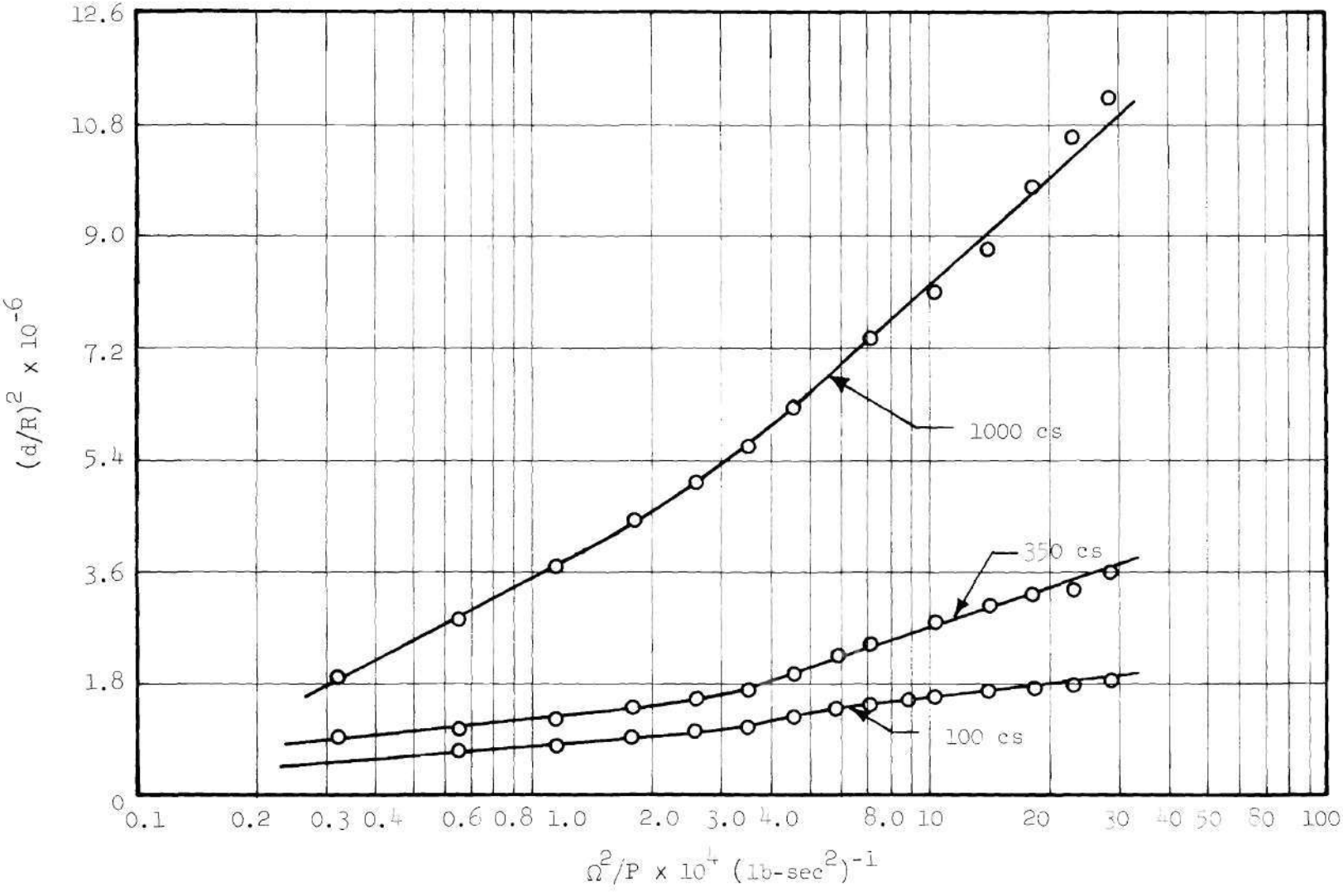

Figure 15. $(d/R)^2$ Versus Ω^2/P for 1000 cs, 350 cs, 100 cs Silicone Fluid.

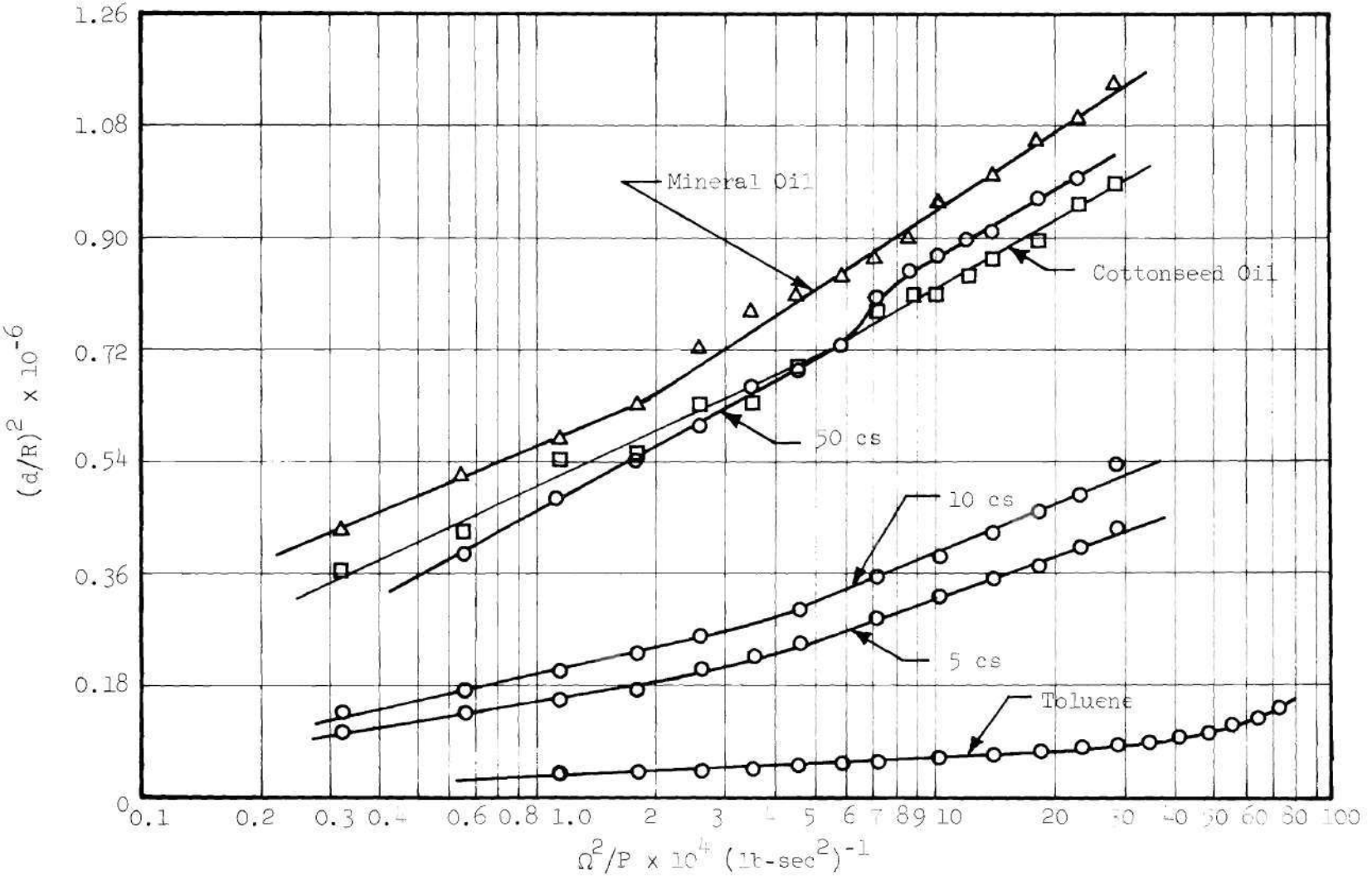

Figure 16. $(d/R)^2$ Versus Ω^2/P For 50 cs, 10 cs, 5 cs Silicone Fluid, Cottonseed Oil, Mineral Oil, and Toluene.

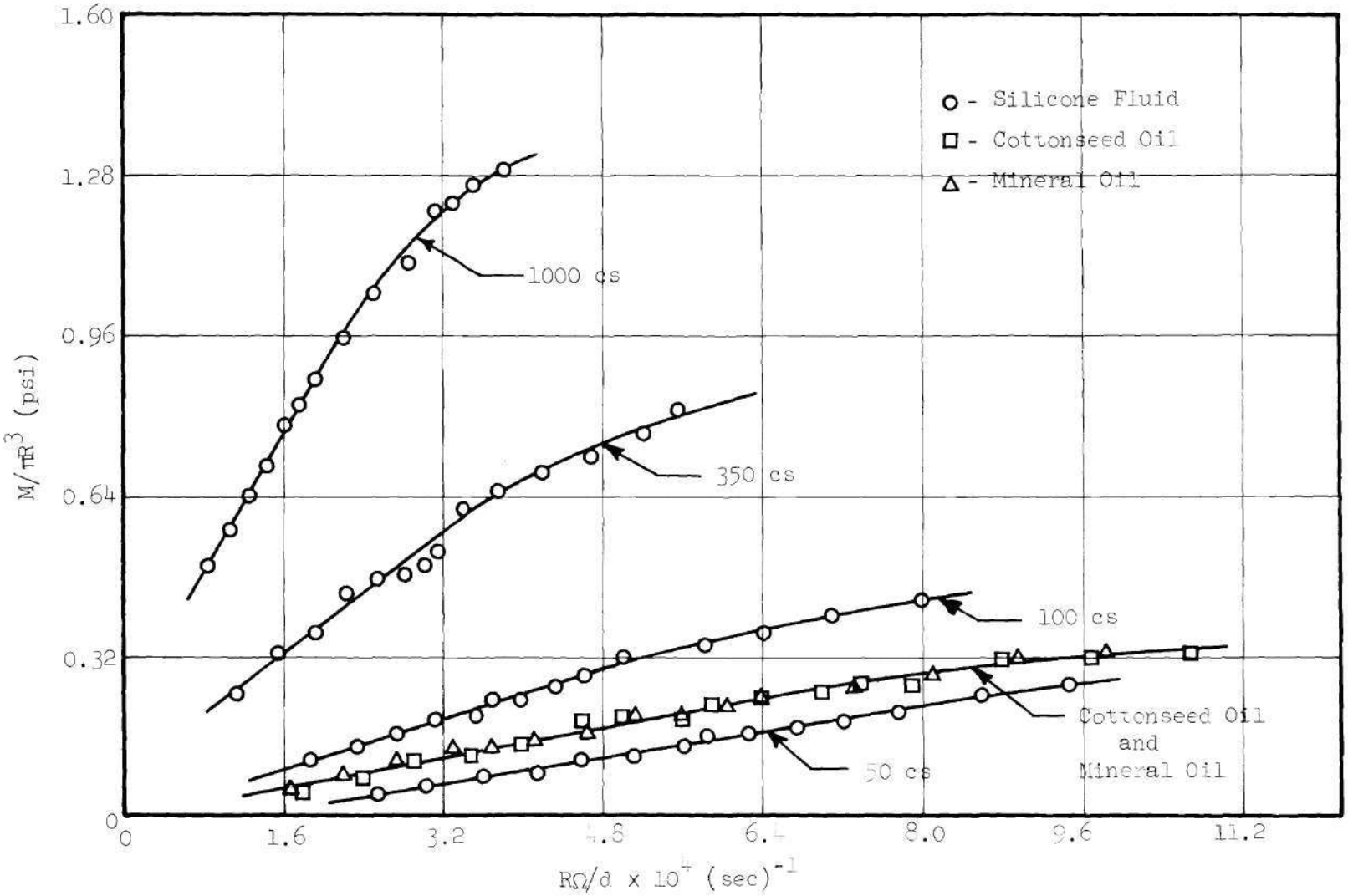

Figure 17. Torque Versus Shear Rate.

Table 1. General Data

Radius of Plates - R = 0.590 inches

Weight of Rotor - P = 0.038 pounds

RPM	Angular Velocity Ω rad/sec	$\Omega/P \times 10^2$ $(lb\text{-}sec)^{-1}$	$\Omega^2/P \times 10^4$ $(lb\text{-}sec^2)^{-1}$
100	10.47	2.8	0.28
105	11.0	2.9	0.32
150	15.7	4.1	0.65
200	20.9	5.5	1.14
250	26.2	6.9	1.79
300	31.4	8.3	2.57
350	36.6	9.6	3.50
400	41.8	11.0	4.56
450	47.0	12.4	5.84
500	52.2	13.7	7.12
550	57.5	15.1	8.73
600	62.7	16.5	10.26
650	68.0	17.9	12.10
700	73.2	19.3	13.99
800	83.6	22.0	18.25
900	94.0	24.7	23.07
1000	104.7	27.6	28.60
1100	115.0	30.3	34.4
1200	125.2	33.0	41.0
1300	136.0	35.8	48.2
1400	146.6	38.6	55.5
1500	157.1	41.3	64.2
1600	167.5	44.1	72.7

Table 2. Experimental Data for 1000cs Silicone Fluid
Dielectric Constant $\epsilon = 2.73$

Clockwise Rotation

RPM	Gap Thickness $d \times 10^{-3}$ inches	Torque M in-lb	Temperature ^{o}F
105	0.85	0.33	76.0
150	0.94	0.39	76.5
200	1.02	0.45	78.0
250	1.09	0.51	78.0
300	1.16	0.54	79.0
350	1.23	0.57	80.0
400	1.30	0.60	81.0
500	1.41	0.67	82.0
600	1.44	0.72	85.0
700	1.49	0.74	87.0
800	1.54	0.84	89.5
900	1.57	0.86	91.5
1000	1.61	0.91	93.0
1100	1.61	0.93	96.0

Counter Clockwise Rotation

105	0.89	0.30	78.5
150	1.03	0.35	78.5
200	1.24	0.38	79.0
250	1.38	0.41	80.0
300	1.48	0.46	81.0
350	1.57	0.49	81.0
400	1.63	0.50	82.0
500	1.79	0.56	83.5
600	1.92	0.64	86.0
700	2.00	0.68	87.5
800	2.10	0.70	89.5
900	2.27	0.73	92.5
1000	2.35	0.75	93.5
1100	2.43	0.76	96.5

(Continued)

Table 2. Experimental Data for 1000cs Silicone Fluid
Dielectric Constant $\epsilon = 2.73$ (Continued)

Average

RPM	Average Gap Thickness $\bar{d} \times 10^{-3}$ inches	$\left(\frac{\bar{d}}{R}\right)^2 \times 10^{-6}$	$\frac{M}{\pi R^3}$ psi	Shear Rate $R\Omega/\bar{d} \times 10^4$ sec^{-1}	$\mu\Omega/P$ in^{-2}
105	0.87	2.18	0.50	0.86	5.9
150	0.99	2.82	0.57	1.08	8.3
200	1.13	3.68	0.64	1.26	11.2
250	1.24	4.42	0.70	1.44	14.0
300	1.32	5.00	0.78	1.62	16.9
350	1.40	5.63	0.82	1.78	19.5
400	1.47	6.21	0.87	1.92	22.3
500	1.60	7.35	0.95	2.22	27.8
600	1.68	8.10	1.04	2.52	33.5
700	1.75	8.79	1.10	2.84	39.2
800	1.82	9.51	1.21	3.12	44.7
900	1.92	10.60	1.22	3.32	50.1
1000	1.98	11.20	1.26	3.58	56.0
1100	2.02	11.72	1.29	3.86	61.5

Table 3. Experimental Data for 350cs Silicone Fluid

Dielectric Constant - $\varepsilon = 2.73$

Clockwise Rotation

RPM	Gap Thickness $d \times 10^{-3}$ inches	Torque M in-lb	Temperature ^{o}F
105	0.63	0.11	81.0
150	0.69	0.16	81.0
200	0.71	0.20	81.0
250	0.75	0.23	81.0
300	0.79	0.24	81.0
350	0.83	0.25	84.0
400	0.87	0.26	84.0
450	0.92	0.29	85.0
500	0.93	0.37	87.0
600	0.98	0.39	87.0
700	1.01	0.41	89.0
800	1.03	0.43	91.0
900	1.06	0.46	92.5
1000	1.07	0.48	94.0

Counterclockwise Rotation

105	0.51	0.20	77.0
150	0.54	0.26	77.0
200	0.59	0.28	77.0
250	0.65	0.35	78.5
300	0.68	0.36	80.5
350	0.73	0.37	81.0
400	0.78	0.38	81.5
450	0.86	0.39	82.0
500	0.90	0.43	83.0
600	0.99	0.45	84.0
700	1.06	0.47	85.0
800	1.09	0.49	86.0
900	1.09	0.53	89.0
1000	1.17	0.55	90.0

(Continued)

Table 3. Experimental Data for 350cs Silicone Fluid (Continued)

Average

RPM	Average Gap Thickness $d \times 10^{-3}$ inches	$\left(\frac{d}{R}\right)^2 \times 10^{-6}$	$\frac{M}{\pi R^3}$ psi	Shear Rate $R\Omega/d \times 10^4$ sec^{-1}	$\mu\Omega/P$ in^{-2}
105	0.57	0.92	0.25	1.16	2.1
150	0.61	1.06	0.33	1.55	2.9
200	0.65	1.21	0.37	1.93	3.9
250	0.70	1.41	0.45	2.24	4.9
300	0.74	1.55	0.47	2.56	5.9
350	0.78	1.72	0.48	2.82	6.8
400	0.82	1.95	0.50	3.04	7.8
450	0.89	2.27	0.53	3.16	8.8
500	0.92	2.41	0.62	3.41	9.7
600	0.99	2.79	0.65	3.78	11.7
700	1.03	3.07	0.68	4.21	13.7
800	1.06	3.22	0.71	4.71	15.6
900	1.07	3.30	0.76	5.22	17.6
1000	1.12	3.59	0.81	5.57	19.6

Table 4. Experimental Data for 100cs Silicone Fluid

Dielectric Constant $\epsilon = 2.72$

Clockwise Rotation

RPM	Gap Thickness $d \times 10^{-3}$ inches	Torque M in-lb	Temperature °F
100	0.478	0.03	76.5
150	0.540	0.05	76.5
200	0.563	0.06	76.5
250	0.603	0.09	77.0
300	0.634	0.10	77.0
350	0.655	0.11	77.0
400	0.682	0.12	77.0
450	0.704	0.13	77.5
500	0.718	0.15	78.0
550	0.722	0.16	79.0
600	0.725	0.18	80.0
700	0.736	0.20	81.0
800	0.742	0.22	82.0
900	0.751	0.25	84.0
1000	0.755	0.27	84.5

Counterclockwise Rotation

105	0.438	0.07	70.0
150	0.467	0.09	70.0
200	0.500	0.11	70.0
250	0.531	0.12	71.0
300	0.560	0.14	71.5
350	0.579	0.16	72.0
400	0.652	0.18	73.0
450	0.691	0.18	73.5
500	0.714	0.18	74.0
550	0.742	0.20	76.0
600	0.750	0.22	77.5
700	0.745	0.24	80.0
800	0.798	0.26	81.0
900	0.809	0.27	83.0
1000	0.809	0.28	84.0

(Continued)

Table 4. Experimental Data for 100cs Silicone Fluid (Continued)

Average

RPM	Average Gap Thickness $d \times 10^{-3}$ inches	$\left(\frac{d}{R}\right)^2 \times 10^{-6}$	$\frac{M}{\pi R^3}$ psi	Shear Rate $R\Omega/d \times 10^{4}$ sec^{-1}	$\mu\Omega/P \times 10^{-1}$ in^{-2}
150	0.504	0.73	0.11	1.88	8.3
200	0.532	0.81	0.14	2.34	11.1
250	0.567	0.92	0.17	2.75	13.9
300	0.597	1.02	0.19	3.13	16.8
350	0.617	1.10	0.20	3.54	19.4
400	0.667	1.28	0.23	3.72	22.2
450	0.698	1.40	0.23	4.00	25.1
500	0.712	1.46	0.26	4.33	27.7
550	0.732	1.54	0.28	4.63	30.5
600	0.738	1.57	0.31	5.01	33.3
700	0.741	1.58	0.34	5.83	39.0
800	0.770	1.70	0.37	6.41	44.4
900	0.781	1.75	0.40	7.10	49.9
1000	0.782	1.76	0.43	8.00	55.8

Table 5. Experimental Data for 50cs Silicone Fluid

Dielectric Constant $\epsilon = 2.69$

Clockwise Rotation

RPM	Gap Thickness $d \times 10^{-3}$ inches	Torque M in-lb	Temperature ^{o}F
115	0.379	0.01	77.0
150	0.412	0.02	77.0
200	0.447	0.03	77.0
250	0.480	0.05	77.0
300	0.495	0.06	77.0
350	0.516	0.07	77.0
400	0.525	0.08	77.5
450	0.538	0.08	77.5
500	0.551	0.08	77.5
550	0.565	0.10	78.0
600	0.578	0.10	78.0
650	0.582	0.10	78.5
700	0.582	0.12	79.0
800	0.588	0.13	80.0
900	0.594	0.14	81.0

Counterclockwise Rotation

105	0.309	0.03	77.0
150	0.326	0.05	77.0
200	0.373	0.05	77.0
250	0.390	0.05	77.0
300	0.411	0.06	77.5
350	0.438	0.07	78.0
400	0.449	0.08	79.0
450	0.462	0.11	79.5
500	0.511	0.12	80.5
550	0.521	0.13	80.5
600	0.524	0.14	81.0
650	0.533	0.15	81.5
700	0.540	0.15	82.0
800	0.567	0.17	83.0
900	0.587	0.19	84.0

(Continued)

Table 5. Experimental Data for 50cs Silicone Fluid (Continued)

Average

RPM	Average Gap Thickness $d \times 10^{-3}$ inches	$\left(\frac{d}{R}\right)^2 \times 10^{-6}$	$\frac{M}{\pi R^3}$ psi	Shear Rate $R\Omega/d \times 10^4$ sec^{-1}	$\mu\Omega/P \times 10^{-1}$ in^{-2}
150	0.369	0.39	0.05	2.56	4.1
200	0.410	0.48	0.06	3.05	5.5
250	0.435	0.54	0.08	3.61	6.9
300	0.453	0.59	0.09	4.14	8.3
350	0.477	0.66	0.11	4.59	9.6
400	0.487	0.68	0.12	5.12	11.0
450	0.500	0.72	0.14	5.62	12.4
500	0.531	0.81	0.16	5.85	13.7
550	0.543	0.85	0.17	6.29	15.1
600	0.551	0.87	0.18	6.76	16.5
650	0.558	0.89	0.19	7.24	17.9
700	0.561	0.91	0.21	7.75	19.3
800	0.578	0.96	0.24	8.60	22.0
900	0.591	1.00	0.26	9.46	24.7

Table 6. Experimental Data for 10cs Silicone Fluid

Dielectric Constant $\epsilon = 2.61$

Clockwise Rotation

RPM	Gap Thickness $d \times 10^{-3}$ inches	Temperature °F
105	0.242	73
150	0.282	73
200	0.296	73
250	0.316	73
300	0.340	73
350	0.360	73
400	0.360	73
450	0.380	73
500	0.392	73
600	0.407	73
700	0.415	73
800	0.435	74
900	0.440	74
1000	0.465	74

Counterclockwise Rotation

105	0.194	72
150	0.220	72
200	0.232	72
250	0.250	72
300	0.260	72
400	0.286	72
500	0.315	72
600	0.325	73
700	0.351	73
800	0.363	73
900	0.380	73
1000	0.398	73

(Continued)

Table 6. Experimental Data for 10cs Silicone Fluid (Continued)

Average

RPM	Average Gap Thickness $d \times 10^{-3}$ inches	$\left(\frac{d}{R}\right)^2 \times 10^{-6}$	Shear Rate $R\Omega/d \times 10^{4}$ sec^{-1}	$\mu\Omega/P \times 10^{-1}$ in^{-2}
105	0.218	0.138	2.98	0.57
150	0.251	0.172	3.69	0.80
200	0.264	0.201	4.67	1.08
250	0.283	0.230	5.46	1.35
300	0.300	0.259	6.18	1.63
400	0.323	0.299	7.64	2.16
500	0.353	0.359	8.73	2.69
600	0.366	0.385	10.11	3.23
700	0.383	0.422	11.28	3.78
800	0.399	0.456	12.36	4.31
900	0.410	0.483	13.53	4.84
1000	0.432	0.537	14.30	5.41

Table 7. Experimental Data for 5cs Silicone Fluid

Dielectric Constant $\epsilon = 2.47$

Clockwise Rotation

RPM	Gap Thickness $d \times 10^{-3}$ inches	Temperature ^{o}F
105	0.189	74
150	0.214	74
200	0.232	74
250	0.250	74
300	0.262	74
350	0.282	74
400	0.296	74
500	0.316	74
600	0.334	74
700	0.348	74
800	0.358	74
900	0.372	74
1000	0.386	74

Counterclockwise Rotation

105	0.188	74
150	0.208	74
200	0.232	74
250	0.240	74
300	0.272	74
350	0.280	74
400	0.292	74
500	0.314	74
600	0.334	74
700	0.350	74
800	0.358	74
900	0.370	74
1000	0.386	74

(Continued)

Table 7. Experimental Data for 5cs Silicone Fluid (Continued)

Average

RPM	Average Gap Thickness $d \times 10^{-3}$ inches	$\left(\frac{d}{R}\right)^2 \times 10^{-3}$	Shear Rate $R\Omega/d \times 10^{4}$ sec^{-1}	$\mu\Omega/P \times 10^{-1}$ in^{-2}
105	0.189	0.103	3.44	0.28
150	0.211	0.129	4.35	0.39
200	0.232	0.155	5.34	0.53
250	0.245	0.172	6.20	0.66
300	0.267	0.204	7.10	0.80
350	0.281	0.227	7.70	0.92
400	0.294	0.247	8.38	1.06
500	0.315	0.284	9.81	1.32
600	0.334	0.322	11.14	1.58
700	0.349	0.351	12.47	1.85
800	0.358	0.368	13.85	2.11
900	0.371	0.396	15.00	2.37
1000	0.386	0.428	16.06	2.65

Table 8. Experimental Data for Mineral Oil

Dielectric Constant $\epsilon = 2.23$

Viscosity 83cs ($77^{\circ}F$)

Clockwise Rotation

RPM	Gap Thickness $d \times 10^{-3}$ inches	Torque M in-lb	Temperature $^{\circ}F$
105	0.41	0.03	77.0
150	0.44	0.06	77.0
200	0.48	0.06	77.0
250	0.49	0.08	77.0
300	0.53	0.09	77.0
350	0.54	0.09	77.0
400	0.55	0.11	77.0
450	0.56	0.12	77.5
500	0.59	0.13	77.5
550	0.59	0.14	78.0
600	0.59	0.15	79.0
700	0.60	0.17	80.0
800	0.62	0.19	80.5
900	0.62	0.20	81.5
1000	0.62	0.21	82.5

Counterclockwise Rotation

105	0.37	0.04	77.0
150	0.40	0.06	77.0
200	0.41	0.07	77.0
250	0.44	0.09	77.0
300	0.46	0.10	77.0
350	0.49	0.11	77.0
400	0.50	0.10	77.0
450	0.52	0.13	77.0
500	0.51	0.14	77.5
550	0.53	0.15	77.5
600	0.56	0.15	78.0
700	0.58	0.17	79.0
800	0.60	0.17	79.5
900	0.62	0.19	80.0
1000	0.63	0.20	81.0

(Continued)

Table 8. Experimental Data for Mineral Oil (Continued)

Average

RPM	Average Gap Thickness $d \times 10^{-3}$ inches	$\left(\frac{d}{R}\right)^2 \times 10^{-6}$	$\frac{M}{\pi R^3}$ psi	Shear Rate $R\Omega/d \times 10^4$ sec^{-1}	$\mu\Omega/P \times 10^{-1}$ in^{-2}
105	0.39	0.43	0.06	1.67	4.2
150	0.42	0.52	0.09	2.21	5.9
200	0.45	0.58	0.11	2.74	7.9
250	0.47	0.63	0.14	3.29	9.9
300	0.50	0.72	0.14	3.71	12.0
350	0.52	0.78	0.15	4.16	13.8
400	0.53	0.80	0.17	4.66	15.8
450	0.54	0.83	0.20	5.14	17.9
500	0.55	0.86	0.20	5.60	19.7
550	0.56	0.89	0.22	6.06	21.7
600	0.58	0.95	0.23	6.40	23.8
700	0.59	1.01	0.26	7.32	27.8
800	0.61	1.06	0.28	8.10	31.7
900	0.62	1.09	0.31	8.96	35.6
1000	0.63	1.15	0.33	9.82	39.7

Table 9. Experimental Data for Cottonseed Oil

Dielectric Constant $\epsilon = 3.14$
Viscosity $\mu = 59$cs (77°F)
Clockwise Rotation

RPM	Gap Thickness $d \times 10^{-3}$ inches	Torque M in-lb	Temperature $^{\circ}$F
105	0.38	0.02	76.0
150	0.42	0.03	76.0
200	0.46	0.05	76.0
250	0.47	0.07	76.0
300	0.49	0.09	76.0
350	0.50	0.10	76.0
400	0.52	0.11	76.0
450	0.53	0.13	76.5
500	0.54	0.13	76.5
550	0.55	0.15	76.5
600	0.55	0.15	76.5
650	0.56	0.17	77.0
700	0.57	0.19	77.0
800	0.57	0.20	79.0
900	0.58	0.21	80.0
1000	0.58	0.22	81.0

Counterclockwise Rotation

105	0.34	0.04	72.0
150	0.36	0.07	72.0
200	0.39	0.08	72.5
250	0.41	0.09	72.5
300	0.44	0.10	73.0
350	0.44	0.14	73.0
400	0.46	0.15	73.5
450	0.48	0.13	74.0
500	0.50	0.14	74.0
550	0.50	0.16	74.5
600	0.51	0.16	75.5
650	0.52	0.18	76.0
700	0.52	0.17	77.0
800	0.55	0.20	77.5
900	0.57	0.19	78.0
1000	0.57	0.21	79.5

(Continued)

Table 9. Experimental Data for Cottonseed Oil (Continued)

Average

RPM	Average Gap Thickness $d \times 10^{-3}$ inches	$\left(\frac{d}{R}\right)^2 \times 10^{-6}$	$\frac{M}{\pi R^3}$ psi	Shear Rate $R\Omega/d \times 10^4$ sec^{-1}	$\mu\Omega/P \times 10^{-1}$ in^{-2}
105	0.36	0.37	0.05	1.8	3.1
150	0.39	0.43	0.08	2.4	4.3
200	0.43	0.55	0.11	2.9	5.8
250	0.44	0.55	0.12	3.5	7.3
300	0.47	0.63	0.14	4.0	8.8
350	0.47	0.63	0.19	4.6	10.2
400	0.49	0.69	0.20	5.0	11.7
450	0.50	0.72	0.19	5.6	13.1
500	0.52	0.78	0.22	5.9	14.5
550	0.53	0.80	0.23	6.4	16.0
600	0.53	0.80	0.25	7.0	17.5
650	0.54	0.83	0.26	7.4	19.0
700	0.55	0.86	0.26	7.9	20.5
800	0.56	0.89	0.31	8.8	23.3
900	0.57	0.95	0.31	9.7	26.2
1000	0.58	0.98	0.33	10.7	29.3

Table 10. Experimental Data for Toluene

Dielectric Constant $\epsilon = 2.38$

Clockwise Rotation

RPM	Gap Thickness $d \times 10^{-3}$ inches	Temperature $^{\circ}F$
200	0.131	76
250	0.139	76
300	0.145	76
350	0.150	76
400	0.155	76
450	0.160	76
500	0.162	76
600	0.171	76
700	0.177	76
800	0.183	76
900	0.188	76
1000	0.192	76
1100	0.194	76
1200	0.198	76
1300	0.209	76
1400	0.221	76
1500	0.228	76
1600	0.233	76

Counterclockwise Rotation

200	0.088	76
250	0.091	76
300	0.095	76
350	0.101	76
400	0.105	76
450	0.111	76
500	0.113	76
600	0.122	76
700	0.127	76
800	0.133	76
900	0.142	76
1000	0.152	76
1100	0.160	76
1200	0.167	76
1300	0.171	76
1400	0.178	76
1500	0.188	76
1600	0.188	76

(Continued)

Table 10. Experimental Data for Toluene (Continued)

Average RPM	Average Gap Thickness $d \times 10^{-3}$ inches	$\left(\frac{d}{R}\right)^2 \times 10^{-6}$	Shear Rate $R\Omega/d \times_1 10^4$ sec^{-1}	$\mu\Omega/P \times_2 10^{-3}$ in^{-2}
200	0.110	0.035	11.2	6.6
250	0.115	0.037	13.4	8.3
300	0.120	0.040	15.4	10.0
350	0.126	0.046	17.1	11.5
400	0.130	0.049	19.0	13.2
450	0.136	0.052	20.4	14.9
500	0.138	0.055	22.3	16.4
600	0.147	0.063	25.2	19.8
700	0.152	0.066	28.4	23.2
800	0.158	0.072	31.2	26.4
900	0.165	0.078	33.6	29.6
1000	0.172	0.086	35.9	33.1
1100	0.177	0.089	38.3	36.4
1200	0.183	0.095	40.4	39.6
1300	0.190	0.103	42.2	43.0
1400	0.200	0.115	43.2	46.3
1500	0.208	0.124	44.6	49.6
1600	0.211	0.144	46.8	52.9

Table 11. Reiner's Experimental Data for Toluene

Dielectric Constant $\epsilon = 2.38$

Viscosity $\mu = 0.0057$ poises

Weight of Rotor P = 0.0365 pounds

Ω rad/sec	$\Omega/P \times 10^{2}$ $(lb\text{-}sec)^{-1}$	$\Omega^{2}/P \times 10^{4}$ $(lb\text{-}sec^{2})^{-1}$	Gap Thickness $d \times 10^{-3}$ inches	$\left(\frac{d}{R}\right)^{2} \times 10^{-6}$	Shear Rate $R\Omega/d \times 10^{4}$ sec^{-1}
58.6	16.1	9.4	0.116	0.039	29.8
61.8	16.9	10.5	0.116	0.039	31.4
72.2	19.8	14.3	0.119	0.041	35.8
73.3	20.1	14.7	0.125	0.045	34.6
94.2	25.8	24.3	0.130	0.049	42.8
104.7	28.7	30.0	0.132	0.051	46.8
125.6	34.4	43.2	0.144	0.060	51.5
146.6	40.2	59.0	0.150	0.065	57.7
167.5	45.9	76.8	0.156	0.070	63.3
188.5	51.6	97.4	0.159	0.073	70.0
209.4	57.4	120.0	0.162	0.075	76.3
261.7	71.7	187.0	0.169	0.082	91.4

Weight of Rotor P = 0.0859 pounds

62.8	7.3	4.6	0.107	0.022	34.6
83.8	9.8	8.2	0.115	0.038	43.0
104.7	12.2	12.8	0.121	0.042	51.1
120.4	14.0	16.9	0.123	0.044	57.8
127.7	14.9	19.0	0.124	0.044	60.8
146.6	17.1	25.0	0.130	0.048	66.5
167.5	19.5	32.7	0.137	0.054	72.1
188.5	21.9	41.4	0.144	0.060	77.2
209.4	24.4	51.0	0.152	0.066	81.3
73.3	5.8	4.3	0.108	0.034	40.0
83.8	6.7	5.6	0.111	0.035	44.5
104.7	8.3	8.7	0.118	0.040	52.4
112.0	8.9	10.0	0.122	0.043	54.2
125.6	10.0	12.5	0.123	0.043	60.3
146.6	11.6	17.1	0.127	0.046	68.1
167.5	13.3	22.3	0.133	0.051	74.3
188.5	15.0	28.2	0.136	0.053	81.8
209.4	16.6	34.8	0.140	0.056	88.3
261.7	20.8	54.4	0.147	0.062	105.0

CHAPTER V

SUMMARY OF CONCLUSIONS AND RECOMMENDATIONS

Summary of Conclusions

The silicone fluids and the vegetable oils exhibit visco-elastic properties when sheared at high rates of shear. At lower shear rates these fluids are essentially Newtonian fluids and the cross-stresses found are due to a hydrodynamical viscous wedge effect present in the viscometer.

The cross-stress found in toluene by Reiner, as well as by the author, is strictly a viscous wedge effect and is not a manifestation of viscoelasticity in toluene. However, some doubt must remain as to whether or not toluene possesses viscoelasticity since any weak visco-elastic tendencies would have been masked by the viscous wedge effect. Also there was a slight indication of a linear relationship between $\left(\frac{d}{R}\right)^2$ and $\frac{\Omega^2}{P}$ for very high shear rates in the results obtained in this work.

The visco-elastic properties of fluids depend not only on the static viscosity of the fluid but also on the molecular structure of the fluid. This was shown by comparing the results for the vegetable oils with the results for the silicone polymer which had a different molecular structure.

Since a firm conclusion could not be made about whether toluene has visco-elastic properties it is not possible to say, based on this one program of research, whether or not Stokesian fluidity effects were present at the very high shear rates developed for toluene.

The simple fluid theory appears to be a reliable model for viscoelastic effects in these fluids even at the high shear rates developed.

Recommendations

It is recommended that any viscometer utilized for additional research be designed so that the film thickness can be kept fixed and that a provision for controlling the temperature be added. Having the film thickness fixed should eliminate the viscous wedge effect, but it would make it impossible to have a self-alignment feature, thus making it necessary to align the plates very accurately.

APPENDIX

SIMPLE FLUID THEORY

The development of Noll's theory of simple fluids (5) is given for completeness.

Preliminary Definitions

The mechanics of continuous media is concerned with the motion and deformation of bodies, consisting of material points X. In the course of a motion these material points change their position in space. Let $\underline{x}$ be the position in Euclidean space of the material point X at time t, where t represents the present time. At time τ, $\tau \leq t$, this same material point X occupied the position $\underline{\xi}$ in Euclidean space. The function $\underline{\chi}_t$, called the relative deformation function, expresses the dependence of $\underline{\xi}$ on $\underline{x}$, t, and τ as

$$\underline{\xi} = \underline{\chi}_t(\underline{x}, \tau) \ . \tag{A.1}$$

The gradient $\underline{F}_t(\tau)$ of $\underline{\chi}_t$ with respect to $\underline{x}$

$$\underline{F}_t(\tau) = \nabla \underline{\chi}_t(\underline{x}, \tau) = \text{grad}_{\underline{x}}\, \underline{\xi} \ , \tag{A.2}$$

is the first deformation gradient of the material point at time τ relative to time t. $\underline{F}_t(\tau)$ is called the relative deformation gradient and it describes the change of local configuration at X between times t and τ.

It is clear that for $\tau = t$, (A.1) reduces to

$$\underline{x} = \underline{\chi}_t(\underline{x}, t) \ . \tag{A.3}$$

Since the gradient of $\underline{x}$ with respect to $\underline{x}$ is the identity tensor $\underline{1}$, the relative deformation gradient

$$\underline{F}_t(t) = \underline{1} \ . \tag{A.4}$$

The tensor function called the history of the relative deformation gradient is defined by

$$\underline{F}(s) = \underline{F}_t(t-s), \ s \geq 0 \ , \tag{A.5}$$

i.e., $\tau = t-s$. This tensor function describes the relation between the local configuration at the present time and the local configuration at s time units in the past. The history $\underline{F}(s)$ depends not only on the choice of the material point X, but also on the choice of the present time t. It follows from (A.4) that the value of the function $\underline{F}(s)$ for $s = 0$ is the identity

$$\underline{F}(0) = \underline{1} \tag{A.6}$$

The velocity $\underline{v} = \underline{v}(\underline{x}, t)$ of the material point whose position at time t is the place $\underline{x}$ is the derivative of the relative deformation function (A.1) with respect to τ, evaluated at $\tau = t$:

$$\underline{v} = \underline{v}(\underline{x}, t) = \frac{d}{d\tau} \underline{\chi}_t(\underline{x}, \tau)\Big|_{\tau=t} \ . \tag{A.7}$$

The acceleration $\underline{a} = \underline{a}(\underline{x}, t)$ is obtained in a similar manner:

$$\underline{a} = \underline{a}(\underline{x},t) = \frac{d^2}{d\tau^2}\,\underline{\chi}_t(\underline{x},t)\Big|_{\tau=t} . \tag{A.8}$$

The gradient of the velocity field $\underline{v} = \underline{v}(x,t)$ will be denoted by

$$\underline{L} = \underline{L}(t) = \nabla\,\underline{v}(\underline{x},t) . \tag{A.9}$$

The symmetric part of the velocity gradient

$$\underline{D} = \frac{1}{2}(\underline{L} + \underline{L}^T) \tag{A.10}$$

is called the stretching or rate of deformation tensor.

A motion is called isochoric if the volume of each part of the body remains unchanged. In a smooth isochoric motion, this is the case if

$$\det \underline{F}_t(\tau) = +1 , \tag{A.11}$$

or equivalently if

$$\mathrm{tr}\underline{D} = \mathrm{div}\,\underline{v} = 0 . \tag{A.12}$$

Any constitutive equation must satisfy the principle of material objectivity. This principle states that any two observers of a motion of a body find the same stress. Another way of saying this is that material properties of a body are invariant with respect to change of frame, i.e. with respect to arbitrary time-dependent, rigid rotations.

It can be proved that every change of frame must be of the form

$$\underline{x}^* = \underline{c} + \underline{Q}(\underline{x} - \underline{q}) , \tag{A.13}$$

where $\underline{c}$ and $\underline{q}$ are points and $\underline{Q}$ is an orthogonal tensor (21). The point $\underline{q}$ can be taken to be independent of the time t, but the point $\underline{c}$ and the orthogonal tensor $\underline{Q}$ are functions of time.

Apply a change of frame to the motion of a body. The point $\underline{x}$ occupied by the particle X at time t and the point $\underline{\xi}$ occupied by X at time τ are transformed into

$$\underline{x}^* = \underline{c}(t) + \underline{Q}(t)\ (\underline{x}-\underline{q}) \tag{A.14}$$

and

$$\underline{\xi}^* = \underline{c}(\tau) + \underline{Q}(\tau)\ (\underline{\xi}-\underline{q})\ , \tag{A.15}$$

respectively. Combining (A.14), (A.15), with (A.1), the following relation between $\underline{\xi}^*$ and $\underline{x}^*$ is obtained:

$$\begin{aligned}\underline{\xi}^* &= \underline{\chi}_t^*(\underline{x}^*, \tau) \\ &= \underline{c}(\tau) + \underline{Q}(\tau)[\underline{\chi}_t(\underline{q} + \underline{Q}(t)^{-1}\{\underline{x}^* - \underline{c}(t)\}, \tau) - \underline{q}]\ .\end{aligned} \tag{A.16}$$

Equation (A.16) gives the relationship of the relative deformation function $\underline{\chi}_t^*$ after the change of frame to the relative deformation function $\underline{\chi}_t$ before the change of frame. Let $\underline{F}_t^*(\tau)$ be the gradient of $\underline{\chi}_t^*(\underline{x}^*, \tau)$ with respect to $\underline{x}^*$,

$$\underline{F}_t^*(\tau) = \nabla \underline{\chi}_t^*(\underline{x}^*, \tau)\ . \tag{A.17}$$

$\underline{F}_t^*(\tau)$ is the relative deformation gradient after the change of frame.

It follows from (A.15) that the gradient of $\underline{\xi}^*$ with respect to $\underline{\xi}$ is $\underline{Q}(\tau)$, and from (A.14) that the gradient of $\underline{x}$ with respect to $\underline{x}^*$ is

$\underline{Q}(t)^{-1}$. Using the chain rule, we infer from (A.17) and (A.2) the relation*

$$\underline{F}^{*}_{t}(\tau) = \underline{Q}(\tau)\underline{F}_{t}(\tau)\underline{Q}(t)^{-1} . \tag{A.18}$$

Putting

$$\underline{R}(s) = \underline{Q}(t-s) , \quad s \geq 0 , \tag{A.19}$$

we conclude from (A.18) and from the orthogonality of $\underline{R}(s)$ that the history (A.5) is transformed by the change of frame into the new history

$$\underline{F}^{*}(s) = \underline{R}(s)\ \underline{F}(s)\ R(0)^{T} . \tag{A.20}$$

Now consider two points $\underline{x}$ and $\underline{y}$ at the same time t. The change of frame (A.13) transforms these points into

$$\underline{x}^{*} = \underline{c} + \underline{Q}(\underline{x}-\underline{q}) ,$$

$$\underline{y}^{*} = \underline{c} + \underline{Q}(\underline{y}-\underline{q}) . \tag{A.21}$$

Taking the point-difference of the two equations (A.21) we obtain

$$\underline{x}^{*} - \underline{y}^{*} = \underline{Q}(\underline{x}-\underline{y}) . \tag{A.22}$$

It follows from (A.22) that in order for representations of a vector $\underline{u}$ by point differences to be preserved under changes of frame, it is necessary that $\underline{u}$ be transformed into

$$\underline{u}^{*} = \underline{Q}\underline{u} . \tag{A.23}$$

---

*$\underline{F}^{*}_{t}(\tau) = \text{grad}_{\underline{x}}{}^{*}\ \underline{\xi}^{*} = \text{grad}_{\underline{\xi}}\ \underline{\xi}^{*}\ \text{grad}_{\underline{x}}\ \underline{\xi}\ \text{grad}_{\underline{x}}{}^{*}\ \underline{x} = \underline{Q}(\tau)\underline{F}_{t}(\tau)\underline{Q}(t)^{-1}$

Since $\underline{Q}$ is orthogonal, if follows from (A.23) that a change of frame preserves distances and angles. It follows, in particular, that the unit normal vector of a surface element must obey the transformation rule (A.23), i.e.,

$$\underline{n}^* = \underline{Q}\,\underline{n} \ . \tag{A.24}$$

Assuming that the geometrical relation between the surface element and the stress vector $\underline{t}$ is also preserved under changes of frame, $\underline{t}$ transforms into

$$\underline{t}^* = \underline{Q}\,\underline{t} \ . \tag{A.25}$$

Combining (A.24), (A.25) with the fact that the stress vector can be expressed in the form $\underline{t} = \underline{T}\,\underline{n}$, where $\underline{T}$ is the stress tensor, we find

$$\underline{t}^* = \underline{T}^*\underline{n}^* \ , \tag{A.26}$$

where

$$\underline{T}^* = \underline{Q}\,\underline{T}\,\underline{Q}^{-1} = \underline{Q}\,\underline{T}\,\underline{Q}^{T} \tag{A.27}$$

Equation (A.27) shows how the stress tensor transforms under a change of frame. Using the notation of (A.19) and regarding $\underline{T}$ to be the stress tensor at time t, (A.27) takes the form

$$\underline{T}^* = \underline{R}(0)\underline{T}\,R(0)^{T} \ . \tag{A.28}$$

The Simple Visco-elastic Fluid

Noll's theory of simple fluids (5) is based upon the very general concept that only the past and present motion can determine the present

stress. That is, the constitutive equation of a simple fluid requires that the stress be determined by the deformation history, i.e., the set of the first deformation gradients of the motion taken between the configuration at a time s in the past and the present configuration as reference. A simple fluid is also defined as a material which has the greatest possible material symmetry, that is, the material response of a fluid is the same in every configuration and it has no preferred or natural configuration. The stress in a fluid in equilibrium must reduce to a hydrostatic pressure since a fluid is a substance capable of flow.

The constitutive equation of a simple fluid, in view of the facts stated above, is given in the form

$$\underline{T} + p\,\underline{1} = \underset{s=0}{\overset{\infty}{\underline{\mathcal{K}}}}(\underline{F}(s)) , \tag{A.29}$$

where p is the hydrostatic pressure, $(\underline{F}(s))$ is the history and $\underline{\mathcal{K}}$ is a functional. In order to make this fluid an incompressible fluid only isochoric motions are permitted, thus we have the additional constitutive equation

$$\det(\underline{F}(s)) = 1 . \tag{A.30}$$

The pressure p now becomes an indeterminant hydrostatic pressure.

The tensor on the left of (A.29) is called the extra stress and is denoted by $\underline{T}_E$:

$$\underline{T}_E = \underline{T} + p\,\underline{1} . \tag{A.31}$$

The functional $\underline{\mathcal{K}}$ in (A.29) embodies the dependence of the extra

stress on the history, $\underline{F}(s)$. The mechanical behavior of a fluid is characterized by this functional which is different for each simple fluid.

The form of this functional is restricted by the principle of material objectivity. For a broad class of flows encompassing essentially all of the shear flows of classical hydrodynamics, geometric constraints allow a reduction of this functional to a function. For this class of flows, the non-linear stresses are then expressed in terms of three material functions which are functions of the deformation rate. This was shown by Coleman and Noll (8). These flows are called viscometric flows.

Because of the indeterminate pressure p in (A.29), that equation does not suffice to assign a unique functional $\underline{\mathcal{K}}$ to each material. This non-uniqueness can be removed by some convention such as

$$\operatorname{tr} \underline{T}_E = \operatorname{tr} \underline{\mathcal{K}}_{s=0}^{\infty} (\underline{F}(s)) = 0 . \tag{A.32}$$

If this convention is used, then p is identical with the mean pressure, i.e.,

$$p = -\frac{1}{3} \operatorname{tr} \underline{T} . \tag{A.33}$$

To see that the constitutive equation (A.30) satisfies the principle of material objectivity, observe that, by (A.20),

$$\begin{aligned} \det \underline{F}^*(s) &= \det (\underline{R}(s)\, \underline{F}(s)\, \underline{R}(o)^T) \\ &= \det \underline{R}(s) \det \underline{R}(o) \det \underline{F}(s) . \end{aligned} \tag{A.34}$$

Since every orthogonal tensor is unimodular and since $\underline{R}(s)$ is orthogonal and depends continuously on s, we find that

$$\det \underline{R}(s) = \det \underline{R}(o) = \pm 1 \ . \tag{A.35}$$

It is seen by combining (A.34) and (A.35) that

$$\det \underline{F}^{*}(s) = \det \underline{F}(s) \ , \tag{A.36}$$

which proves that (A.30) is preserved by changes of frame.

If the constitutive equation (A.29) satisfies the principle of material objectivity, it must remain valid if $\underline{T}$ and $\underline{F}(s)$ are replaced by their transforms $\underline{F}^{*}$ and $\underline{F}^{*}(s)$ under a change of frame:

$$\underline{T}^{*} + p\underline{1} = \underset{s=o}{\overset{\infty}{\mathcal{H}}} (\underline{F}^{*}(s)) \ . \tag{A.37}$$

Substitution of (A.20) and (A.28) into (A.37) gives

$$\underline{R}(0)\underline{T}\ \underline{R}(0)^{T} + p\underline{1} = \underline{R}(0)(\underline{T} + p\underline{1})\underline{R}(0)^{T}$$

$$= \underset{s=o}{\overset{\infty}{\mathcal{H}}} (\underline{R}(s)\underline{F}(s)\ \underline{R}(0)^{T}) \ . \tag{A.38}$$

Substitution of (A.29) into (A.38) yields

$$\underline{R}(0)\ \underset{s=o}{\overset{\infty}{\mathcal{H}}} (\underline{F}(s))\underline{R}(0)^{T} = \underset{s=o}{\overset{\infty}{\mathcal{H}}} (\underline{R}(s)\ \underline{F}(s)\ \underline{R}(0)^{T}) \ . \tag{A.39}$$

The principle of material objectivity requires that (A.39) be satisfied for every continuous function $\underline{R}(s)$ whose values are orthogonal tensors and for every history $\underline{F}(s)$. Thus in order for a functional $\underline{\mathcal{H}}$ to be the defining functional of a simple fluid the functional relation (A.39) must be satisfied.

Consider now the steady torsional shear flow. The contravariant components of the velocity field in a cylindrical coordinate system are

assumed to be

$$v^r = 0 , \quad v^\theta = \omega(z) , \quad v^z = 0 . \tag{A.40}$$

The flow defined by (A.40) is the flow shown in Figure 1a, where $\omega(z)$ is the velocity profile at a given radius r.*

Having prescribed the velocity field, it is possible to calculate the relative deformation function

$$\underline{\xi} = \underline{\chi}_t(\underline{x}, \tau) = \underline{\xi}(\tau) \tag{A.41}$$

from a knowledge of $\underline{v}(\underline{x},t)$. The velocity of the material point X at time τ is the derivative $\dot{\underline{\xi}}(\tau)$ with respect to τ. Since at time τ the material point X has the position $\underline{\xi}(\tau)$, its velocity at that time is equal to $\underline{v}(\underline{\xi}(\tau), \tau)$. Thus, $\underline{\xi}(\tau)$ must satisfy the differential equation

$$\dot{\underline{\xi}}(\tau) = \underline{v}(\underline{\xi}(\tau), \tau) . \tag{A.42}$$

On the other hand, it follows from (A.41) and (A.3) that

$$\underline{\xi}(t) = \underline{x} . \tag{A.43}$$

Thus, the relative deformation function (A.41) is simply that solution of (A.42) which satisfies the initial condition (A.43).

For the velocity field (A.40) the vector differential equation (A.42) became

$$\dot{\xi} = 0 , \quad \dot{\eta} = \omega(\zeta) , \quad \dot{\zeta} = 0 , \tag{A.44}$$

*In physical components the velocity field is given by

$$v^{<r>} = 0 , \quad v^{<\theta>} = r\omega(z) , \quad v^{<z>} = 0 .$$

where $\xi = \xi(\tau)$, $\eta = \eta(\tau)$ and $\zeta = \zeta(\tau)$ are the coordinates of $\underline{\xi} = \underline{\xi}(\tau)$. The condition (A.43) is equivalent to

$$\xi(t) = r \ , \quad \eta(t) = \theta \ , \quad \zeta(t) = z \ , \tag{A.45}$$

where r, θ, z are the coordinates of $\underline{x}$. It follows from $(A.44)_{1,3}$ and $(A.45)_{1,3}$ that

$$\xi = \xi(\tau) \equiv r \ , \quad \zeta = \zeta(\tau) \equiv z \tag{A.46}$$

hold for all values of τ. Substituting $(A.46)_2$ into $(A.44)_2$ we find

$$\dot{\eta} = \omega(z) \ . \tag{A.47}$$

Integrating (A.47) using $(A.45)_2$ and the fact that $\omega(z)$ does not depend on τ, we find that

$$\eta = \eta(\tau) = \omega(z)(\tau - t) + \theta \ . \tag{A.48}$$

The equations (A.46) and (A.48) give the coordinates of the relative deformation function (A.41). The matrix of the physical components of the relative deformation gradient $\underline{F}_t(\tau)^*$ becomes

$$[\underline{F}_t(\tau)] = \begin{Vmatrix} 1 & 0 & 0 \\ 0 & 1 & r\omega'(z)(\tau - t) \\ 0 & 0 & 1 \end{Vmatrix} \ . \tag{A.49}$$

It follows from (A.49) that the history (A.5) has the form

$$\underline{F}(s) = \underline{1} - s\,\underline{M} \ , \tag{A.50}$$

---

*$F_t(\tau)^{\alpha}_{\beta} = \xi^{\alpha}_{,\beta}$ where the comma indicates partial differentiation.

where $\underline{M}$ is the tensor with the time-independent matrix

$$[\underline{M}] = \begin{Vmatrix} 0 & 0 & 0 \\ 0 & 0 & \kappa \\ 0 & 0 & 0 \end{Vmatrix} , \qquad (A.51)$$

where $\kappa = r\omega'(z)$. (A.30) holds for (A.50), i.e., torsional shear flow is an isochoric motion.

Substituting the history (A.50) into the constitutive equation (A.29), we obtain

$$\underline{T} + p\underline{1} = \underline{T}_E = \underset{s=0}{\overset{\infty}{\underline{\mathcal{H}}}} (\underline{1} - s\,\underline{M}) = \underline{h}(\underline{M}) , \qquad (A.52)$$

where $\underline{h}(\underline{M})$ is a tensor-valued function of the constant tensor $\underline{M}$. To see this reduction one must remember that a functional is a function whose value is determined by all possible values of its argument function. In this particular case, equation (A.29) says that the stress is determined by the values of the tensor $\underline{F}(s)$ at all times past. Now, for this particular flow, $\underline{F}(s)$ has the form given by (A.50). Thus $\underline{\mathcal{H}}$ is a functional, whose value is determined by the values of the tensor $\underline{F}(s)$ at all past times, but the tensor $\underline{F}(s)$ at any past time is determined by $\underline{M}$, and the past-time, so the net result of all this determination is that $\underline{\mathcal{H}}$ must be equal, for this flow,* to a certain function $\underline{h}$ of $\underline{M}$, where $\underline{M}$ depends only on the variable κ.

Now the identity (A.39), in the case where $\underline{F}(s)$ is given by (A.50) and $\underline{R}(s) \equiv \underline{Q}$ where Q is independent of s, becomes

*In general it can be shown that this is true for the class of flows known as viscometric flows (8).

$$\underline{Q}\ \underline{h}(\underline{M})\underline{Q}^{T} = \underline{h}(\underline{Q}\ \underline{M}\ \underline{Q}^{T}) \ , \tag{A.53}$$

for all orthogonal tensors $\underline{Q}$. Any function satisfying an identity of the form (A.53) is called an isotropic function. Thus, for a history of the form (A.50), the extra stress is an isotropic function of $\underline{M}$.

First consider a reflection in the plane parallel to the flow, i.e., choose $\underline{Q}$ in (A.53) to be the orthogonal tensor whose matrix is

$$[\underline{Q}] = \begin{Vmatrix} -1 & 0 & 0 \\ 0 & 1 & 0 \\ 0 & 0 & 1 \end{Vmatrix} \ . \tag{A.54}$$

A calculation using (A.51) and (A.54) shows that $[\underline{Q}][\underline{M}][\underline{Q}]^{T} = [\underline{M}]$; hence

$$\underline{Q}\ \underline{M}\ \underline{Q}^{T} = \underline{M} \ . \tag{A.55}$$

Thus, for the tensor (A.54), the identity (A.53) reduces to

$$\underline{Q}\ \underline{h}(\underline{M})\underline{Q}^{T} = \underline{h}(\underline{M}) \ . \tag{A.56}$$

Hence the stress tensor $\underline{T} = -\ p\underline{1} + \underline{h}(\underline{M})$ must have the property

$$\underline{Q}\ \underline{T}\ \underline{Q}^{T} = \underline{T} \ . \tag{A.57}$$

Denoting the matrix of the physical components of $\underline{T}$ by

$$[\underline{T}] = \begin{Vmatrix} T^{<rr>} & T^{<r\theta>} & T^{<rz>} \\ T^{<\theta r>} & T^{<\theta\theta>} & T^{<\theta z>} \\ T^{<zr>} & T^{<z\theta>} & T^{<zz>} \end{Vmatrix} \ , \tag{A.58}$$

the matrix $\underline{Q}\ \underline{T}\ \underline{Q}^{T}$ may be calculated from (A.54):

$$[\underline{Q}\,\underline{T}\,\underline{Q}^{T}] = \begin{Vmatrix} T^{<rr>} & -T^{<r\theta>} & -T^{<rz>} \\ -T^{<\theta r>} & T^{<\theta\theta>} & T^{<\theta z>} \\ -T^{<zr>} & T^{<z\theta>} & T^{<zz>} \end{Vmatrix} . \qquad (A.59)$$

It follows from (A.57), (A.58) and (A.59) that

$$T^{<r\theta>} = T^{<\theta r>} = 0 , \quad T^{<rz>} = T^{<zr>} = 0 ; \qquad (A.60)$$

i.e., $[\underline{T}]$ must have the form

$$[\underline{T}] = \begin{Vmatrix} T^{<rr>} & 0 & 0 \\ 0 & T^{<\theta\theta>} & T^{<\theta z>} \\ 0 & T^{<z\theta>} & T^{<zz>} \end{Vmatrix} . \qquad (A.61)$$

This is a necessary condition following from use of a particular $\underline{Q}$, in the identity (A.53). Therefore the matrix of the extra-stress $\underline{T}_E = T+p\underline{1}$ must have the form

$$[\underline{T}_E] = \begin{Vmatrix} T^{<rr>} + p & 0 & 0 \\ 0 & T^{<\theta\theta>} + p & T^{<\theta z>} \\ 0 & T^{<z\theta>} & T^{<zz>} + p \end{Vmatrix} . \qquad (A.62)$$

By (A.52), the extra-stress $\underline{T}_E$, and hence its matrix (A.62), is determined by $\underline{M}$. Therefore, the components of the matrix (A.62) are functions of κ. From the dependence of the shear stress $T^{<\theta z>} = T^{<z\theta>}$ on κ we set

$$T^{<\theta z>} = \tau(\kappa) . \qquad (A.63)$$

Since the diagonal components of the matrix (A.62) determine the normal stress differences $T^{\langle ii\rangle} - T^{\langle kk\rangle}$, these differences are functions of κ. For two of these functions we set

$$T^{\langle zz\rangle} - T^{\langle rr\rangle} = \sigma_1(\kappa) \ , \tag{A.64}$$

$$T^{\langle \theta\theta\rangle} - T^{\langle rr\rangle} = \sigma_2(\kappa) \ . \tag{A.65}$$

The other normal stress differences are expressible as simple combinations of those given in (A.64) and (A.65). Since p is indeterminate, the information contained in (A.63) - (A.65) is equivalent to that contained in constitutive equation (A.29), for this flow.

It has been shown, directly from the principle of material objectivity, that the most general stress system is given by equations (A.63) - (A.65). We have shown that the material properties defined by the functional $\underline{\mathcal{H}}$ reduce, for torsional shear flow, to the three functions τ, σ_1, and σ_2.

The material functions are not fully arbitrary. Apply the principle of material objectivity again for a different $\underline{Q}$, i.e., the tensor whose matrix is

$$[\underline{Q}] = \begin{Vmatrix} 1 & 0 & 0 \\ 0 & -1 & 0 \\ 0 & 0 & 1 \end{Vmatrix} \ . \tag{A.66}$$

A calculation using (A.51) and (A.66) yields $[\underline{Q}][\underline{M}][\underline{Q}^T] = -[\underline{M}]$, and hence

$$\underline{Q}\ \underline{M}\ \underline{Q}^T = -\underline{M} \ . \tag{A.67}$$

Substitution of (A.67) into (A.56) gives

$$\underline{Q}\ \underline{T}_E\ \underline{Q}^T = \underline{Q}\ \underline{h}(\underline{M})\underline{Q}^T = \underline{h}(-\underline{M}) \ . \tag{A.68}$$

The matrix of $\underline{Q}\ \underline{T}_E\ \underline{Q}^T$ becomes, using (A.66) and (A.62):

$$[\underline{Q}\ \underline{T}_E\ \underline{Q}^T] = \begin{Vmatrix} T^{<rr>} + p & 0 & 0 \\ 0 & T^{<\theta\theta>} + p & T^{<\theta z>} \\ 0 & T^{<z\theta>} & T^{<zz>} + p \end{Vmatrix} \ . \tag{A.69}$$

By (A.68), the matrix (A.69) must be the same as the matrix obtained by using $-\underline{M}$ rather than $\underline{M}$ in defining the history (A.50). On the other hand, in view of (A.51), $-\underline{M}$ is obtained from $\underline{M}$ by simply replacing κ by $-\kappa$. Hence, when κ is replaced by $-\kappa$, the shearing stress $T^{<\theta z>}$ changes to $-T^{<\theta z>}$, while the normal stress differences $T^{<zz>} - T^{<rr>}$ and $T^{<\theta\theta>} - T^{<rr>}$ remain unchanged. It follows that

$$\tau(-\kappa) = -\tau(\kappa) \ , \ \sigma_1(-\kappa) = \sigma_1(\kappa) \ , \ \sigma_2(-\kappa) = \sigma_2(\kappa) \ . \tag{A.70}$$

In other words, the shear stress function must be odd and the normal stress functions must be even.

The condition (A.70) is physically reasonable, since replacing κ by $-\kappa$ corresponds to reversing the direction of the flow, hence the condition (A.70), states that the tangential traction must be reversed in order to reverse the flow. The conditions $(A.70)_{2,3}$ state that the differences in the normal tractions remain unaffected by a reversal of the flow.

Since the fluid is at rest when $\kappa = 0$ and the only stress is the

hydrostatic pressure we see that

$$\tau(0) = \sigma_1(0) = \sigma_2(0) = 0 \ . \qquad \text{(A.71)}$$

LITERATURE CITED

1. Weissenberg, K., "A Continuum Theory of Rheological Phenomena," Nature 159, 310-311, 1947.

2. Reiner, M., "A Mathematical Theory of Dilatency," American Journal of Mathematics 67, 350-362, 1945.

3. Rivlin, R. S., "Hydrodynamics of Non-Newtonian Fluids," Nature 160, 611-613, 1947.

4. Rivlin, R. S. and J. L. Ericksen, "Stress-Deformation Relations for Isotropic Materials," Journal of Rational Mechanics and Analysis 4, 323-425, 1955.

5. Noll, W., "A Mathematical Theory of the Mechanical Behavior of Continuous Media," Archive for Rational Mechanics and Analysis 2, 197-226, 1958.

6. Markovitz, H., "Normal Stress Effect in Polyisobutylene Solutions. II. Classifications and Applications of Rheological Theories," Transactions of the Society of Rheology 1, 37-52, 1957.

7. Markovitz, H. and R. B. Williamson, "Normal Stress Effect in Polyisobutylene Solutions. I. Measurements in a Cone and Plate Instrument," Transactions of the Society of Rheology, 25-36, 1957.

8. Coleman, B. D. and W. Noll, "On Certain Steady Flows of General Fluids," Archive for Rational Mechanics and Analysis 3, 289-303, 1959.

9. Markovitz, H. and D. R. Brown, "Parallel Plate and Cone-Plate Normal Stress Measurements on Polyisobutylene-Cetane Solutions," Transactions of the Society of Rheology 7, 137-154, 1963.

10. Merrington, A. C., "Flow of Visco-elastic Materials in Capillaries," Nature 152, 663, 1943.

11. Needs, S. J., "Boundary Film Investigations," Transactions of the ASME, 331-345, May 1940.

12. Reiner, M., "Cross Stresses in the Laminar Flow of Liquids," Physics of Fluids, 3, No. 3, 427-432, 1960.

13. Barlow, A. J. and J. Lamb, "The Visco-elastic Behavior of Lubricating Oils Under Cyclic Shearing Stress," Proceedings of the Royal Society of London Science, A253, 52-69, 1961.

14. Henniker, J. C., "The Depth of the Surface Zone of a Liquid," Reviews of Modern Physics 21, No. 2, 322-450, 1949.

15. Taylor, Sir Geoffrey and P. G. Saffman, "Effects of Compressibility at Low Reynolds Numbers," Journal of the Aeronautical Sciences, 24, No. 8, 553-562, 1957.

16. Greensmith, H. W. and R. S. Rivlin, "The Hydrodynamics of Non-Newtonian Fluids, III. The Normal Stress Effect in High-Polymer Solutions," Philosophical Transactions of the Royal Society (London), A245, 359-428, 1953.

17. Rayleigh, Lord, "Notes on the Theory of Lubrication," Philosophical Magazine 6, XXXV, p. 1, 1918.

18. Radio Formulae, Handbook of Chemistry and Physics, 14th Edition, p. 3255, Chemical Rubber Publishing Co., Cleveland, Ohio.

19. Chemical Products Division, Dow Corning Corporation, Midland, Michigan, Bulletin: 05-145, February 1966.

20. Currie, C. C. and B. F. Smith, "Flow Characteristics of Organopolysiloxane Fluids and Greases," Industrial and Engineering Chemistry, Vol. 42, page 2457, December 1950.

21 Noll, W., "Euclidean Geometry and Minkowskian Chronometry," American Mathematical Monthly 71, 129-144, 1964.

OTHER REFERENCES

1. Coleman, B. D., H. Markovitz, and W. Noll, "Viscometric Flows of Non-Newtonian Fluids," Springer-Verlag, New York, Inc., 1966.

2. Truesdell, C., and R. Toupin, The Classical Field Theories. Handbuch der Physik III/1, Berlin, Göttingen, Heidelberg.

3. Truesdell, C. and W. Noll, The Non-Linear Field Theories of Mechanics. Handbuch der Physik III/3, Berlin, Göttingen, Heidelberg.

VITA

Charles Philip Thomas was born on November 30, 1941 in Limestone County, Alabama. He was educated in the public schools of Limestone County, Alabama, and graduated from East Limestone High School, Limestone County in 1959. Charles entered Auburn University in September 1959, and received a Bachelor of Science in Mechanical Engineering in June 1963. He entered Georgia Tech in September 1963 and received a Master of Science Degree in Engineering Mechanics in June 1965.

Charles is married to the former Carolyn Rebecca Burgess of Dadeville, Alabama and they have a son Alan Ward.